

Reviewed Preprint v1 • September 16, 2025 Not revised

#### **Neuroscience**

# In vivo mapping of striatal neurodegeneration in Huntington's disease with Soma and Neurite Density Imaging

Vasileios Ioakeimidis, Marco Palombo, Chiara Casella, Lucy Layland, Carolyn B McNabb, Robin Schubert, Philip Pallmann, Monica E Busse, Cheney JG Drew, Sundus Alusi, Timothy Harrower, Anne E Rosser, Claudia Metzler-Baddeley

Cardiff University Brain Research Imaging Centre (CUBRIC), School of Psychology, Cardiff University, Cardiff, United Kingdom • Danish Research Centre for Magnetic Resonance, Department for Radiology and Nuclear Medicine, Copenhagen University Hospital Amager and Hvidovre, Copenhagen, Denmark • Department for Forensic and Neurodevelopmental Sciences, Institute of Psychiatry, Psychology and Neuroscience, King's College London, London, United Kingdom • Early life imaging research department, School of Biomedical Engineering and Imaging Sciences, King's College London, London, United Kingdom • London Collaborative Ultra high field System (LoCUS), Kings College London, London, United Kingdom • George Huntington Institut (GHI), Münster, Germany • Centre for Trials Research, School of Medicine, Cardiff University, Cardiff, United Kingdom • The Walton Centre for Neurology and Neurosurgery, Liverpool, United Kingdom • Royal Devon and Exeter NHS Trust, Exeter, United Kingdom • Cardiff University Brain Repair Group, School of Biosciences, Cardiff University, Cardiff, United Kingdom • Advanced Neurotherapeutics Centre (ANTC), Department of Neurology and Psychological Medicine, School of Medicine, Cardiff University, Cardiff, United Kingdom

- d https://en.wikipedia.org/wiki/Open\_access
- © Copyright information

### **eLife Assessment**

This **important** manuscript presents a novel application of the SANDI (Soma and Neurite Density Imaging) model to study microstructural alterations in the basal ganglia of individuals with Huntington's disease (HD). The **compelling** methods, to our understanding, the first application of SANDI to neurodegenerative diseases, provide strong evidence for HD-related neurodegeneration in the striatum, account significantly for striatal atrophy, and correlate with motor impairments. The integration of novel diffusion acquisition and modelling methods with multimodal behavioural data are both of high value in their own right, and create a framework for future studies.

https://doi.org/10.7554/eLife.107661.1.sa4

# **Abstract**



# **Background**

Huntington's Disease (HD) is an inherited neurodegenerative disorder characterised by progressive cognitive and motor decline due to atrophy in basal ganglia networks. No disease-modifying therapies exist, but novel clinical trials are ongoing. Non-invasive imaging biomarkers sensitive to HD neuropathology are essential for evaluating therapeutic effects.

Soma and Neurite Density Imaging (SANDI), a multi-shell diffusion-weighted imaging model, estimates intracellular signal fractions from sphere-shaped soma in grey matter. SANDI-derived apparent soma density and size in the striatum have potential as proxies for HD-related neurodegeneration. While HD is rare, it provides a valuable model for other neurodegenerative diseases due to its clear genetic cause and shared features of protein abnormalities.

# **Objective**

To characterise HD-related microstructural abnormalities in the basal ganglia and thalami using SANDI and examine associations between SANDI indices, volumetric measurements, and motor performance.

# **Methods**

T1-weighted anatomical and multi-shell diffusion-weighted images (b-values: 200–6,000 s/mm²) were acquired using a 3T Siemens Connectom scanner (300mT/m) in 56 premanifest and manifest HD individuals (Mean $_{\rm Age}$  = 46.1, SD $_{\rm Age}$  = 13.8, 25 females) and 57 healthy controls (Mean $_{\rm Age}$  = 45.0, SD $_{\rm Age}$  = 13.8, 31 females). HD participants completed Quantitative Motor (Q-Motor) tasks, including speeded and paced finger tapping, which were reduced to one principal component of motor performance. Following standard diffusion-weighted data preprocessing, SANDI and diffusion tensor models estimated apparent soma density, soma size, neurite density, extracellular signal fraction, fractional anisotropy, and mean diffusivity. The caudate, putamen, pallidum, and thalamus were segmented bilaterally, and microstructural and volumetric indices were extracted and compared. Correlations between SANDI in- dices, Q-Motor performance, and volumetric measures were analysed.

# **Results**

HD was associated with reduced apparent soma density ( $r_{rb}$  = 0.32, p ≤ 0.007) and increased apparent soma size ( $r_{rb}$  = 0.45, p < 0.001) and extracellular signal fraction ( $r_{rb}$  = 0.34, p ≤ 0.003) in the basal ganglia, but not the thalami, with largest effects at manifest stage. No differences were found in apparent neurite density ( $r_{rb}$  = 0.18, p = 0.17). HD-related increases in fractional anisotropy and mean diffusivity in the basal ganglia were replicated. Q-Motor component scores correlated negatively with apparent soma density and positively with soma size and extracellular signal fraction. SANDI indices and age explained up to 63% of striatal atrophy in HD.



# Conclusion

SANDI measures detected HD-related neurodegeneration in the striatum, accounted significantly for striatal atrophy, and correlated with motor impairments. Decreased apparent soma density and increased soma size align with *ex vivo* evidence of medium spiny neuron loss and glial reactivity. SANDI shows promise as an *in vivo* biomarker and surrogate outcome measure in clinical trials of disease-modifying therapies for HD and other neurodegenerative diseases.

# Introduction

Huntington's disease (HD) is an autosomal dominantly inherited neurodegenerative disorder caused by a pathogenic CAG repeat expansion of the Huntingtin gene. HD is characterised by a progressive loss of cognitive and motor functions as well as psychiatric disturbances. The clinical onset of HD is commonly defined by the manifestation of motor symptoms, such as chorea, reduced voluntary motor control, bradykinesia, and difficulty maintaining rhythmic and paced movements. However, changes in the brain, notably striatal atrophy in the basal ganglia may precede the motor onset by up to 24 years may and correlate with motor and cognitive decline. May precede the motor onset by up to 24 years may be and correlate with motor and cognitive decline. While HD is rare (~12 in 100,000), it can be seen as a model neurodegenerative disorder, due to its clear genetic cause, well-characterized disease progression, and shared features of protein abnormalities with more common disorders like Alzheimer's and Parkinson's disease.

There is presently no approved disease-modifying therapy for HD, but numerous clinical trials are underway to test the safety and efficacy of novel therapeutics. The recent surge in potential disease-modifying targets has generated a demand for surrogate outcome measures that are sensitive to HD neuropathology and allow a mechanistic assessment of therapeutic effects on striatal neurodegeneration in a timely manner. Volumetric measurements from non-invasive MRI are known to be sensitive to disease progression 17 color and have been adopted into the recently published Huntington's Disease Integrated Staging System (HD-ISS). However, volumetric measurements do not provide information about the underlying neuropathological tissue changes that lead to striatal atrophy, such as the loss of medium spiny neurons (MSN) and changes in glia cell density and morphology, including enlargement of reactive astrocytes and microglia. 22 color 2,24 color 2,60 color and microglia. 22 color 2,24 color 2,26 color 2,24 color 2,26 color 2,24 color 2,26 color 2,24 color 2,26 color 2,24 color 2,24 color 2,26 color 2,24 color 2,2

Diffusion-weighted Imaging (DWI) is widely used to investigate brain tissue microstructure *in vivo* by exploiting apparent water displacement due to Brownian motion. Amount of Most DWI studies in HD have used diffusion tensor imaging (DTI), which models extracellular water diffusion as a Gaussian tensor and measures diffusion properties such as mean diffusivity (MD) and the degree of diffusion anisotropy (fractional anisotropy; FA). DTI studies in HD have consistently reported increases in MD and FA in striatal grey matter, 30 , 31 to that likely arise from the selective neurodegeneration of medium spiny neuron connections.

Advances in multi-shell and ultra-strong gradient DWI, 32 have enabled increasingly sophisticated biophysical models that require data acquisition over a range of b-values to separate extra-from intracellular diffusion signals. Several approaches that model intraneurite space with cylinders or sticks have been put forward (e.g. Composite and Restricted Model of Diffusion, CHARMED CHARMED



with localised reductions in fibre orientation dispersion in the corpus callosum and basal ganglia capsules. 37 C. However, despite putamen volume loss, no NODDI-based differences in striatal grey matter were detected in gene-positive individuals long before motor onset. 10 C.

Soma And Neurite Density Imaging (SANDI)<sup>38,C,\*</sup> is a novel biophysical diffusion model that extends multi-compartment approaches like NODDI to account for the more complex geometrical architecture of grey matter. SANDI requires multi-shell acquisition protocols with b-values over 3,000 s/mm<sup>2,C,\*</sup> to capture restricted signal fractions from within grey matter soma, which are modelled as geometrical spheres. In this way, SANDI provides estimates of apparent soma density ( $f_{is}$ ) and soma radius ( $f_{is}$ ) in addition to apparent neurite density ( $f_{in}$ ) (modelled with sticks), extracellular signal fraction ( $f_{ec}$ ) and extracellular diffusivity ( $f_{is}$ ). SANDI has been shown to provide highly reproducible and repeatable parameter estimation across grey matter regions in the human brain<sup>39,C,\*</sup> that align closely with its known cyto- and myeloarchitecture. For instance, the gradients of apparent soma density maps were found to closely match those of Brodmann areas in human cortical regions with different soma density profiles,<sup>38,C,\*</sup> and correlated in the mouse brain with cell density distributions from the Allen atlas.<sup>38,C,\*</sup> These findings suggest the potential of the SANDI model for quantifying neurodegenerative processes in the grey matter of the living human brain.

Clinical applications of SANDI are currently limited to multiple sclerosis (MS), where reductions in apparent soma and neurite density and increases in extracellular signal fraction in grey and white matter align with MS-related demyelination, axonal loss, and neurodegeneration. 41 ,42 These microstructural abnormalities have been found to correlate with disease severity, 42 cortical or subcortical atrophy, 41 ,43 and elevated levels of serum neurofilament light chain (NfL), a neuronal cytoplasmic protein marker of axonal damage, 43 that is also sensitive to HD progression. 44 A5 corrected to the progression.

The primary objective of this study was to assess whether SANDI indices were sensitive and specific to microstructural grey matter differences in the basal ganglia, compared with the thalami, in a group of individuals with premanifest and manifest HD relative to healthy controls. Secondary objectives were the exploration of the extent to which any HD-related SANDI differences accounted for basal ganglia atrophy, assessed with volumetric measurements, and performance differences in motor tasks, including speeded and paced finger tapping, known to be associated with striatal atrophy in HD. 46 C Finally, relationships between SANDI differences and disease burden were explored by employing the Huntington's Disease Integrated Staging System (HD-ISS) 21 C and the CAG-Age Product (CAP<sub>100</sub>) score.

# **Materials and methods**

# **Participants**

MRI data from 56 individuals who tested gene-positive for the mutant *huntingtin* allele and 57 healthy age- and sex-matched individuals (healthy controls; HC) were included in the analyses. Thirty-eight of the gene-positive individuals participated in a randomised controlled feasibility trial of HD-DRUM, <sup>48</sup> a remote rhythmic training intervention, with ethical approval from the Wales Research Ethics Committee 2 (REC Reference: 22/WA/0147). <sup>55</sup> Here we report baseline MRI and behavioural data collected prior to randomisation into the trial arms. Additionally, we included MRI data from 18 gene-positive individuals and 18 age-matched HC from a previous study characterising white matter microstructure in premanifest HD (REC Reference: 18/WA/0172). <sup>49</sup> Further, MRI data from 25 age- and sex-matched HC from the Wales Advanced Neuroimaging Database (WAND) Study (REC Reference: 18.08.14.5332RA3) and 14 from the HD-DRUM study were utilised as comparison control. All participants provided written informed consent according to the Declaration of Helsinki prior to taking part in the studies.



HD gene-positive individuals were identified and screened for eligibility in five HD clinics in the UK (Bristol, Birmingham, Cardiff, Exeter, and Liverpool). HC volunteers were recruited from online advertisements on the Cardiff University social network, Viva Engage, or in HD clinics as support partners or family members of individuals with HD. HC participants were also recruited through <a href="Healthwise Wales">Healthwise Wales</a> and by word of mouth. For the WAND study, data collection is reported elsewhere. Social

Individuals over the age of 18 years with a good command of the English language were eligible to participate. Additional inclusion criteria for individuals with HD.48 CM were:

- Positive for the presence of the mutant huntingtin allele (CAG length ≥ 36 repeats) and/or clinical diagnosis of HD.
- Unified Huntington's Disease Rating Scale (UHDRS) Total Functional Capacity (TFC) score between 9 and 13.<sup>51 ™</sup>

#### Exclusion criteria were:

- Contra-indication for MRI (e.g. pacemakers, stents).
- An inability to provide informed consent.
- For HD participants: A history of any other neurological condition.
- For HC: A history of any neurological or psychiatric condition, and/or alcohol or drug abuse, that have been associated with grey matter volume loss.

To characterise general cognitive functioning HD participants were assessed with the Montreal Cognitive Assessment (MOCA).  $^{52}$  Verbal intellectual ability was assessed with the Test of Premorbid Functioning (TOPF).  $^{53}$  Disease burden was estimated by the TFC and the CAG-Age Product (CAP<sub>100</sub>) score,  $^{47}$  which was calculated using the following formula:

$$CAP_{100} = Age * \frac{CAG - 30}{6.49}$$

In addition, HD participants were stratified into one of the four HD-ISS<sup>21</sup> stages using an online calculator (https://enroll-hd.org/calc/html\_basic.htm ):

- Stage 0: Individuals carry a mutated HD gene with CAG repeat  $\geq$  40.
- Stage 1: Individuals meet Stage 0 criteria and exhibit striatal atrophy.
- Stage 2: Individuals meet Stage 1 criteria and exhibit clinical signs or symptoms evidenced by changes in the scores on the United Huntington's Disease Rating Scales (UHDRS). Total Motor Score (TMS) and cognitive changes in the Symbol Digit Modalities Test (SDMT).
- Stage 3: Individuals meet all previous criteria and show signs of functional change in the UHDRS Total Functional Capacity (TFC) score.

# Motor outcome measures

Participants of the HD-DRUM study completed a range of motor tasks from the Quantitative-Motor (Q-Motor) test-battery, 56 C -58 C which has been shown to provide reliable assessments of speeded finger tapping performance in clinical HD trials 59 C ,60 C Tasks included left and right 1) speeded index finger tapping using force transducers, 46 C 2) speeded foot tapping, 3) paced finger tapping and 4) paced foot tapping with a metronome-paced and memory-paced phase, using a fast (0.55s inter-onset interval; IOI) or slow (1.1s IOI) metronome pace as well as 5) 3D pointing to four target locations in a predefined sequence using a position-tracking stylus with the dominant



hand. and 6) 3D target pointing and speeded finger tapping dual task performed with dominant and non-dominant hand, respectively. Outcome measures for the various tasks were as follows:

- Speeded tapping: mean IOI in seconds and mean area under the curve (AUC) in Newtonseconds.
- Paced tapping: mean absolute deviation from the metronome rhythm, measured in seconds.
- Target pointing task: target frequency in Hertz (Hz).
- Target pointing-speeded tapping dual task: target frequency in Hz, mean IOI in seconds, and mean AUC in Newton-seconds.

# **Image acquisition**

MRI data were acquired on a 3T Siemens Connectom scanner (Siemens Healthcare, Erlangen, Germany) with ultra-strong magnetic gradients (300mT/m) at Cardiff University Brain Research Imaging Centre (CUBRIC).

T1-weighted (T1w) images were acquired using a magnetisation-prepared 180-degrees radio-frequency pulses and rapid gradient-echo (MPRAGE), with the following parameters: repetition time (TR) 2,300 ms, echo time (TE) 2 ms, field of view (FOV) 256 x 256 x 192 mm, matrix size 256 x 256 x 192, resolution 1 x 1 x 1 mm $^3$ , flip angle 9°, inversion time (TI) 857 ms, in-plane acceleration (GeneRalised Autocalibrating Partial Parallel Acquisition; GRAPPA) factor 2, phase-encoding direction anterior to posterior (AP), and acquisition time of 6 minutes.

Multi-shell High Angular Resolution Diffusion Imaging (HARDI) $^{62}$  data were obtained at b-values of 200 s/mm² (20 directions), 500 s/mm² (20 directions), 1,200 s/mm² (30 directions). 2,400 s/mm² (61 directions), 4,000 s/mm² (61 directions) and 6,000 s/mm² (61 directions) using a single-shot spin-echo, echo-planar imaging sequence with TR = 3,000 ms, TE = 59 ms, FOV 220 x 200 mm in-plane; matrix size 110 x 110 x 66; 2 mm³ resolution, gradient pulse duration -  $\delta$  = 7 ms, gradient pulses separation -  $\Delta$  = 24 ms in AP phase-encoding direction with an in-plane acceleration (GRAPPA) factor of 2. Fifteen non-diffusion-weighted (b-value = 0 s/mm²) images were acquired [two initial and 11 interspersed at the 33<sup>rd</sup> volume and every 20<sup>th</sup> volume thereafter in AP direction and 2 images in the posterior-to-anterior (PA) direction]. The HARDI acquisition time was 18 minutes.

# **Image processing**

# Diffusion-weighted image preprocessing

Multi-shell HARDI data were pre-processed and corrected for signal drift, susceptibility-induced distortions, motion and eddy current-induced distortions, gradient non-uniformity and Gibbs ringing artifacts using a custom in-house pipeline comprising tools from the FMRIB Software Library (FSL version 6.0.3), 63 the MRtrix software package, 64 the ExploreDTI (version 4.8.6) and in-house MATLAB-based scripts. 39 the MRTrix software package, 64 the ExploreDTI (version 4.8.6) and in-house MATLAB-based scripts.

The FSL brain extraction tool 63 was used to mask the first non-diffusion-weighted image from each phase-encoding direction to exclude non-brain data. The diffusion-weighted MRI volumes were fitted to temporally interspersed b0 volumes to correct for within-image intensity drift by using custom code in MATLAB R2017b (MathWorks Inc., Natick, Massachusetts, USA). Slicewise outlier detection (SOLID) was applied with modified Z-score thresholds of 3.5 (lower) and 10 (upper), utilising a variance-based intensity metric. FSL's top-up tool 67 1,68 was used to estimate susceptibility-induced off-resonance fields from b0 images that were acquired in opposing phase-



For the purpose of comparing our results with the previous literature, 30°C DTI was fitted with ExploreDTI using data with b-values of 500 s/mm² and 1,200 s/mm² to produce outcome maps for FA and MD, estimated with linearly weighted least squares regression.

# **SANDI** analysis

The model fitting produced maps of the intra-neurite, extracellular and intra-soma signal fractions  $(f_{in}, f_{ec}, f_{is})$ , apparent soma size (rs; measured in  $\mu$ m) and intra- and extra-neurite diffusivities  $(D_{in}, D_e;$  measured in mm²/ms). Post-hoc sensitivity analysis of the SANDI model parameters revealed very low sensitivity to changes in  $D_{in}$ . Consequently, it was excluded from further analysis.

# T1-weighted image preprocessing

The default FreeSurfer [74.02] (v6) recon-all pipeline was utilised to segment subcortical basal ganglia ROIs of the caudate, putamen, and globus pallidum as well as of the thalamus as control ROIs. ROIs were segmented from T1w images and were identified and labelled in each hemisphere.

# Extraction of microstructural metrics from regions-of-interest

Median values of each microstructural index from DTI (FA, MD) and SANDI ( $f_{is}$ ,  $f_{in}$ ,  $f_{ec}$ ,  $r_s$ ,  $D_e$ ) models were extracted for each ROI using FSL's *fslmaths*. ROI masks were aligned with the diffusion space using rigid transformation with FSL's *flirt*<sup>75</sup> before eroding the boundaries of the subcortical masks to minimise partial volume effects and then aligning all microstructural maps with the masks.

Volumetric measures for each ROI and intra-cranial volume (ICV) were extracted from FreeSurfer v6. ROI volumes were normalised for ICV. The addition of brain volumes allowed exploration of the extent to which any HD-related SANDI differences accounted for basal ganglia atrophy.

#### Statistical analysis

Statistical analyses were performed in JASP (v0.18.1.0). R version 4.4.1 (2024-06-14). In R-studio (2024.9.0.375). and SPSS (v27) (IBM Corp). Data normality was assessed using the Shapiro-Wilk test, with p < 0.05 indicating non-normal distribution. Descriptive statistics for each group were reported as percentages (%), means and standard deviations (SD). Medians of each microstructural index in each ROI were compared between the groups with Mann-Whitney-U tests because of lack of normality and unequal variance between groups. Effect sizes for group comparisons were therefore reported with rank biserial correlation ( $r_{rb}$ ). Multiple comparisons were corrected with Benjamini-Hochberg's method to control a false discovery rate (FDR) of  $0.05^{80}$  and applied to all statistical tests that related to the same theoretical inference.



Hierarchical linear regression analyses were conducted to test for microstructural SANDI predictors of the variance in volumetric measurements. Regression analyses were carried out for each ROI and each group separately. HD data were modelled by firstly accounting for age and TFC scores (available for all HD participants) simultaneously. This was followed by step-wise inclusion of the SANDI indices using an iterative forward selection and backward elimination method based on each variable's F-statistic and p-value that aimed to maximise the adjusted R²-value while keeping only the most significant predictors. HC data were modelled in the same way except for the inclusion of TFC scores.

Principal Component Analysis (PCA) was carried out to reduce the dimensionality of HD participants' Q-Motor data and hence the number of multiple correlations with microstructural SANDI indices. PCA followed established guidelines to limit the number of extracted components in relatively small sample sizes. Pirst the Kaiser criterion of including all components with an eigenvalue greater than 1 was applied and the Cattell scree plot was inspected to identify the minimal number of components that accounted for most variability in the data. Each extracted component was then assessed for interpretability. PCA was conducted using orthogonal Varimax rotation of the component matrix with Kaiser normalization. Loadings that were greater than 0.5 were considered to be statistically significant.

Spearman's rho ( $\rho$ ) correlations were then calculated between HD participants' motor component scores and the CAP<sub>100</sub> with the SANDI indices, DTI, and volumetric measures in each ROI.

Finally, analyses to explore HD-ISS related differences in SANDI indices were conducted for SANDI indices in the basal ganglia. For these exploratory analyses a binary split combining Stage 0 and Stage 1 as "premanifest" and Stage 2 and Stage 3 as "manifest" was performed, and SANDI indices were collapsed across hemispheres by averaging. Pairwise comparisons between premanifest and HC, premanifest and manifest, and manifest and HC were conducted using Mann–Whitney U tests without additional FDR correction.

# **Results**

# **Demographics**

Information for HD-ISS calculation was available for 27 individuals. N = 9 were stratified into Stage 1, N = 5 into Stage 2, and N = 12 into Stage 3. One individual could not be classified due to their clinical pattern not conforming with the assumption of the HD-ISS model of motor symptoms preceding functional impairments. Twenty-nine individuals could not be classified due to missing clinical data or due to their CAG repeats falling between 36-39. Details of the demographic and clinical information per HD-ISS stage and for participants who could not be classified are summarised in **Supplementary Table 1**.

**Table 2** ☑ displays descriptive statistics for the Q-Motor measures of the HD gene-positive participants.

# **Imaging analysis**

Table 1.

# Demographic and clinical information of participants

	HD group			HC group	Statistic (p-value)	
	N	Mean (SD)	N	Mean (SD)		
Age	56	46.12 (13.79)	57	44.96 (13.75)	t(111) = 0.446 (0.657)	
Female, N (%)		25 (44.7%)		31 (54.4%)	$\chi^2 = 1.073 (0.300)$	
Education (years)	38	14.16 (2.58)	14	15.86 (2.54)	$t_{(50)} = 2.06 (0.448)$	
HD-ISS stage 0/1/2/3, N		0/9/5/12				
MOCA	55	26.47 (3.55)		-		
TOPF	56	49.70 (13.16)		-		
UHDRS-TFC	56	12.11 (1.25)		-		
UHDRS-TMS	51	11.03 (15.82)		-		
CAG	50	41.82 (2.67)		-		
CAP	50	80.55 (22.60)		-		
SDMT	38	45.47 (14.91)				

Abbreviations: CAG: Cytosine Adenine Guanine; CAP: CAG-Age-Product; HC: Healthy Controls; HD: Huntington's Disease; HD-ISS: Huntington's Disease International Staging System; MOCA: Montreal Cognitive Assessment; SD: Standard Deviation; SDMT: Symbol Digit Modalities Test; TFC: Total Functional Capacity; TMS: Total Motor Score; TOPF: Test Of Premorbid Functioning; UHDRS: United Huntington's Disease Rating Scale

Table 2.

# **Descriptive statistics for motor outcome measures**

	HD group			
Task Outcome measure	N	Mann (SD)		
Speeded tapping	N I	Mean (SD)		
Left finger; Area under the curve (N-s)	38	0.13 (0.20)		
Right finger; Area under the curve (N-s)	38	0.07 (0.09)		
Left finger; Inter-onset interval (s)	38	0.26 (0.12)		
Right finger; Inter-onset interval (s)	38	0.23 (0.08)		
Left foot; Inter-onset interval (s)	37	0.37 (0.20)		
Right foot; Inter-onset interval (s)	38	0.35 (0.18)		
Metronome tapping; Absolute deviation from pace (s)	36	0.33 (0.18)		
Left finger; Paced; Fast	38	0.07 (0.06)		
Left finger; Paced; Slow	38	. ,		
	38	0.13 (0.14)		
Left finger; Unpaced; Fast	38	0.07 (0.07)		
Left finger; Unpaced; Slow		0.15 (0.15)		
Right finger; Paced; Fast	38	0.07 (0.06)		
Right finger; Paced; Slow	38	0.13 (0.12)		
Right finger; Unpaced; Fast	38	0.08 (0.06)		
Right finger; Unpaced; Slow	38	0.16 (0.17)		
Left foot; Paced; Fast	36	0.07 (0.05)		
Left foot; Paced; Slow	35	0.16 (0.13)		
Left foot; Unpaced; Fast	36	0.08 (0.09)		
Left foot; Unpaced; Slow	35	0.17 (0.14)		
Right foot; Paced; Fast	37	0.08 (0.04)		
Right foot; Paced; Slow	37	0.16 (0.12)		
Right foot; Unpaced; Fast	37	0.09 (0.09)		
Right foot; Unpaced; Slow	37	0.16 (0.13)		
Pointing (dominant hand)				
Target frequency over trial (Hz)	38	2.62 (0.65)		
Pointing (dominant) and tapping (non-dominant)				
Finger tapping area under the curve (coefficient of variation %)	38	0.76 (0.37)		
Finger tapping area under the curve (N-s)	38	0.31 (0.43)		
Finger tapping inter-onset interval (s)	38	0.39 (0.19)		
Frequency over trial (Hz)	38	3.08 (1.07)		
Pointing target frequency over trial (Hz)	38	2.62 (0.66)		

Abbreviations: Hz: Hertz; N: Newton; s: Seconds



# HD-related differences in volumetric measures

# HD-related differences in microstructural measures

Descriptive and statistical microstructural results are shown in detail in **Table 4** . **Figure 2** provides effect size mappings and raincloud plots of the different microstructural measures for each ROI comparing the two groups.

Regarding the DTI measures, increased FA and MD (FDR-p < 0.01) were observed in the basal ganglia (**Fig. 2E-F**  $\square$ ) with the exception of MD in the left pallidum (FDR-p = 0.854).

No differences were found in the thalami for any of the microstructural metrics.

# Correlations between BG microstructure and motor performance in HD

# **Motor measures**

PCA extracted one principal component that explained 64% of the Q-Motor data with high loadings (> 0.5 or <-0.5) from all variables (**Table 5**  $\square$ ). Spearman's rho correlation between Q-motor component scores and the disease burden CAP<sub>100</sub> score revealed a positive correlation ( $\rho$  = 0.61, p = 0.002, N = 24), i.e., higher disease burden was associated with higher scores in the Q-Motor component reflecting slower and less accurate motor performance (**Figure 3**  $\square$ ).

Spearman's rho correlations between Q-motor component scores and SANDI microstructural measures from all ROIs and scatter plots are displayed in Figure 4. Figure 5. displays correlations and scatter plots of the Q-Motor component with DTI and volumetric indices. Overall, negative correlations were observed between principal Q-Motor component scores and apparent soma density in the basal ganglia, apparent soma size in the pallidum, and volumetric measurements in all ROIs, reflecting that lower apparent soma density and volumes were associated with impaired motor performance, reflected as higher scores in the Q-Motor component. Conversely, positive correlations were present between Q-Motor component scores and apparent soma size, extracellular signal fraction, and extracellular diffusivity in the basal ganglia, i.e. larger apparent soma size and extracellular signal were associated with impaired motor performance (Figure 4. and 5).

# Figure 1.

# Volumetric differences in the basal ganglia and thalamus between HD-gene positive (HD) individuals and healthy controls (HC).

Regions-of-interest (ROIs) were segmented using FreeSurfer v6. All ROIs, except the left thalamus, showed significantly smaller volumes in the HD cohort after FDR correction for multiple comparisons. Colours indicate the strength of rankbiserial correlations  $(r_{rb})$  from Mann-Whitney U tests: Red = strong effect  $(r_{rb} \ge 0.5)$ , Yellow = medium effect  $(0.3 \le r_{rb} < 0.5)$ , White = small effect ( $r_{rh}$  < 0.3). Raincloud plots show the distribution of the volumetric measures in each ROI per group with orange (HD gene=1) for HD-gene positive and green (HD gene=0) for HD-gene negative participants. \* p < 0.05; \*\*\* p < 0.001

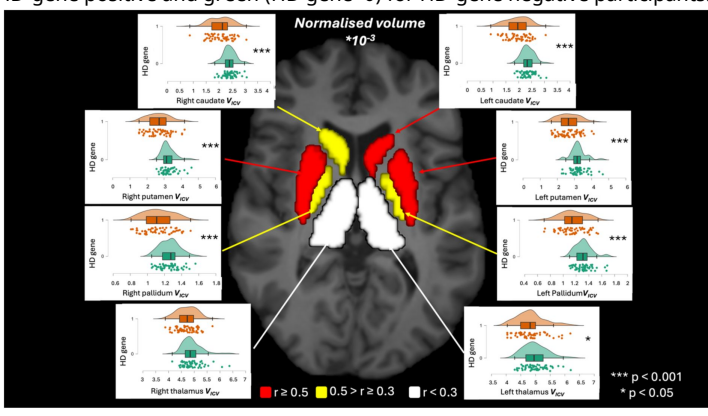


Table 3. Descriptive and Mann-Whitney Statistics for Intracranial Volume-Normalised Regions of Interest

		HD group	HC group	Statistic (FDR-p, effect size)
Region of interest	L/R	Mean (SD)	Mean (SD)	U (p, rank-biserial correlation)
Caudate	L	1.95a (0.45a)	2.352 (0.242)	2464 (<0.001, 0.544)
	R	2.06a (0.43a)	2.41° (0.25°)	2376 (<0.001, 0.489)
Putamen	L	2.67a (0.62a)	3.22a (0.46a)	2397 (<0.001, 0.502)
	R	2.67a (0.66a)	3.25° (0.40°)	2479 (<0.001, 0.553)
Pallidum	L	1.15a (0.20a)	1.32° (0.13°)	2382 (<0.001, 0.492)
	R	1.13a (0.17a)	1.26a (0.12b)	2323 (<0.001, 0.456)
Thalamus	L	4.83° (0.49°)	4.99ª (0.41b)	1955 (0.063, 0.224)
	R	4.72a (0.39a)	4.91° (0.40°)	1981 (0.048, 0.241)

| R | 4.72° (0.39°) | 4.91° (0.40°) | 1981 (0.048, 0.241)

Abbreviations: FDR: False Discovery Rate; HC: Healthy Controls; HD: Huntington's Disease; L: Left Hemisphere; R: Right Hemisphere; SD: Standard Deviation

Multiplied by 10³

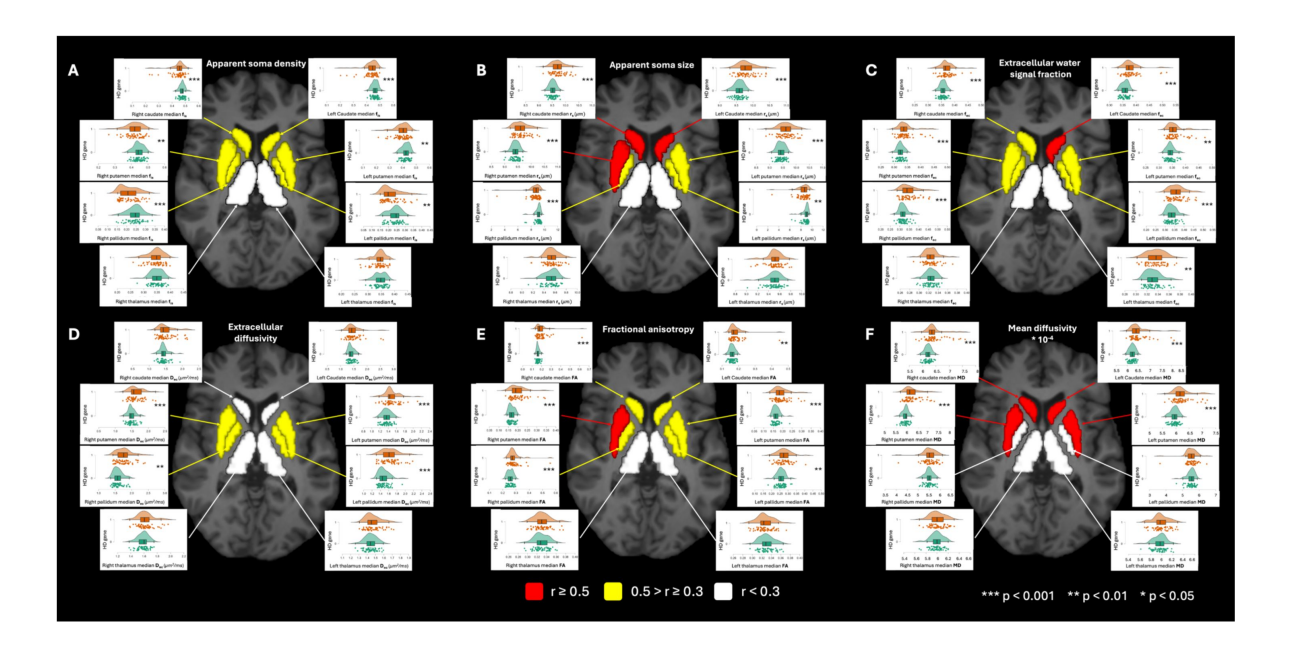


Figure 2.

# Microstructural differences in ROIs between HDgene positive (HD) and healthy control (HC) groups.

Median values of each microstructural measure were extracted per ROI. **A)** HD individuals show reduced soma density  $(f_{is})$  in the basal ganglia (BG). **B)** Soma radius  $(r_s)$  is elevated in the caudate and putamen but reduced in the pallidum. **C)** Extracellular water fraction  $(f_{ec})$  is increased in BG regions in the HD group. **D)** Extracellular diffusivity  $(D_e)$  is higher in the putamen and pallidum. **E)** Fractional anisotropy (FA) is elevated in the BG, and **F)** mean diffusivity (MD) is increased in the striatum. Colours indicate the strength of rank-biserial correlations  $(r_{rb})$  from Mann-Whitney U tests: Red = strong effect  $(r_{rb} \ge 0.5)$ , Yellow = medium effect  $(0.3 \le r_{rb} < 0.5)$ , White = small effect  $(r_{rb} < 0.3)$ . Raincloud plots show the distribution of the microstructural measures in each ROI per group with orange (HD gene=1) for HD-gene positive and green (HD gene=0) for HD-gene negative participants. \* p < 0.05; \*\* p < 0.01; \*\*\* p < 0.001

Table 4. Descriptive and Mann-Whitney Statistics for Microstructural Measures in Regions of Interest

			HD group	HC group	Statistic (FDR-p, effect size)
Microstructural measure	Region of interest	L/R	Mean (SD)	Mean (SD)	U (p, rank-biserial correlation)
Apparent soma density	Caudate	L	0.43 (0.05)	0.46 (0.02)	2227 (<0.001, 0.395)
,		R	0.45 (0.05)	0.48 (0.02)	2318 (<0.001, 0.452)
	Putamen	L	0.39 (0.05)	0.42 (0.03)	2140 (0.003, 0.341)
	T dedition	R	0.42 (0.05)	0.44 (0.03)	2099 (0.007, 0.315)
	Pallidum	L	0.21 (0.05)	0.24 (0.04)	2187 (0.001, 0.370)
	T dinddii	R	0.21 (0.05)	0.24 (0.04)	2249 (<0.001, 0.409)
	Thalamus	L	0.34 (0.03)	0.34 (0.02)	1692 (0.701, 0.060)
	maamas	R	0.35 (0.03)	0.35 (0.02)	1661 (0.776, 0.041)
Apparent soma size	Caudate	L	9.80 (0.25)	9.58 (0.15)	746 (<0.001, -0.533)
Apparent soma size	Condite	R	9.72 (0.25)	9.52 (0.12)	751 (<0.001, -0.529)
	Putamen	I I	9.61 (0.29)	9.43 (0.15)	885 (<0.001, -0.445)
	rutumen	R	9.63 (0.27)	9.40 (0.14)	791 (<0.001, -0.504)
	Pallidum	L		8.88 (0.58)	2126 (0.004, 0.332)
	Palliaum		8.41 (1.08)		
	71.1	R	8.59 (0.94)	9.05 (0.45)	2300 (<0.001, 0.447)
	Thalamus	L	9.51 (0.14)	9.50 (1.32)	1502 (0.701, -0.059)
		R	9.54 (0.13)	9.52 (0.12)	1515 (0.723, -0.051)
Extracellular water signal fraction	Caudate	L	0.38 (0.04)	0.36 (0.01)	757 (<0.001, -0.526)
		R	0.37 (0.02)	0.36 (0.01)	984 (<0.001, -0.383)
	Putamen	L	0.36 (0.03)	0.34 (0.02)	1048 (0.003, -0.343)
		R	0.34 (0.03)	0.32 (0.01)	892 (<0.001, -0.441)
	Pallidum	L	0.36 (0.04)	0.33 (0.02)	910 (<0.001, -0.430)
		R	0.35 (0.04)	0.32 (0.02)	932 (<0.001, -0.416)
	Thalamus	L	0.34 (0.02)	0.33 (0.01)	1294 (0.130, -0.189)
		R	0.33 (0.01)	0.32 (0.01)	1636 (0.853, 0.025)
Extracellular diffusivity	Caudate	L	1.47 (0.28)	1.40 (0.11)	1420 (0.418, -0.110)
		R	1.51 (0.25)	1.44 (0.13)	1482 (0.633, -0.071)
	Putamen	L	1.47 (0.17)	1.36 (0.11)	902 (<0.001, -0.435)
		R	1.62 (0.20)	1.49 (0.11)	1002 (0.001, -0.372)
	Pallidum	L	1.62 (0.20)	1.48 (0.12)	842 (<0.001, -0.472)
		R	1.76 (0.23)	1.59 (0.14)	809 (<0.001, -0.493)
	Thalamus	L	1.47 (0.07)	1.44 (0.07)	1411 (0.394, -0.116)
		R	0.31 (0.03)	0.31 (0.03)	1377 (0.305, -0.137)
Apparent neurite density	Caudate	L	0.18 (0.04)	0.17 (0.02)	1514 (0.723, -0.051)
		R	0.18 (0.05)	0.16 (0.02)	1317 (0.167, -0.175)
	Putamen	1	0.24 (0.04)	0.23 (0.03)	1374 (0.303, -0.139)
	7 444111011	R	0.23 (0.04)	0.23 (0.03)	1411 (0.394, -0.116)
	Pallidum	1 i	0.41 (0.05)	0.42 (0.03)	1553 (0.854, -0.027)
	ramouni	R	0.43 (0.05)	0.43 (0.03)	1473 (0.605, -0.078)
	Thalamus	1	0.31 (0.03)	0.31 (0.03)	1565 (0.868, -0.019)
	Indiamas	R	0.31 (0.03)	0.31 (0.03)	1459 (0.554, -0.086)
Fractional anisotropy	Caudate	L	0.18 (0.04)	0.16 (0.02)	993 (0.001, -0.378)
rracиonal anisotropy	Caudate				
		R	0.20 (0.07)	0.16 (0.02)	889 (<0.001, -0.443)
	Putamen	L	0.19 (0.04)	0.17 (0.02)	873 (<0.001, -0.453)
		R	0.20 (0.04)	0.17 (0.02)	710 (<0.001, -0.555)
	Pallidum	L	0.28 (0.04)	0.26 (0.03)	1115 (0.010, -0.301)
		R	0.28 (0.05)	0.26 (0.02)	995.5 (<0.001, -0.401)
	Thalamus	L	0.33 (0.02)	0.33 (0.02)	1808 (0.319, 0.133)
		R	0.33 (0.02)	0.33 (0.02)	1532 (0.776, -0.040)
Mean diffusivity	Caudate	L	6.50a (0.41a)	6.23a (0.13a)	777.5 (<0.001, -0.513)
		R	6.44a (0.36a)	6.20a (0.12a)	760.5 (<0.001, -0.523)
	Putamen	L	6.22a (0.34a)	5.95* (0.15*)	653.5 (<0.001, -0.591)
		R	6.20a (0.34a)	5.91a (0.13a)	624.5 (<0.001, -0.609)
	Pallidum	L	5.54a (0.36a)	5.51a (0.23a)	1557.5 (0.854, -0.024)
		R	5.52a (0.30a)	5.49a (0.18a)	1437 (0.474, -0.100)
	Thalamus	L	5.98a (0.14a)	5.96ª (0.11ª)	1509 (0.721, -0.055)

Abbreviations: FDR: False Discovery Rate; HC: Healthy Controls; HD: Huntington's Disease; L: Left Hemisphere; R: Right Hemisphere; SD: Standard Deviation \*: Multiplied by 10<sup>4</sup>

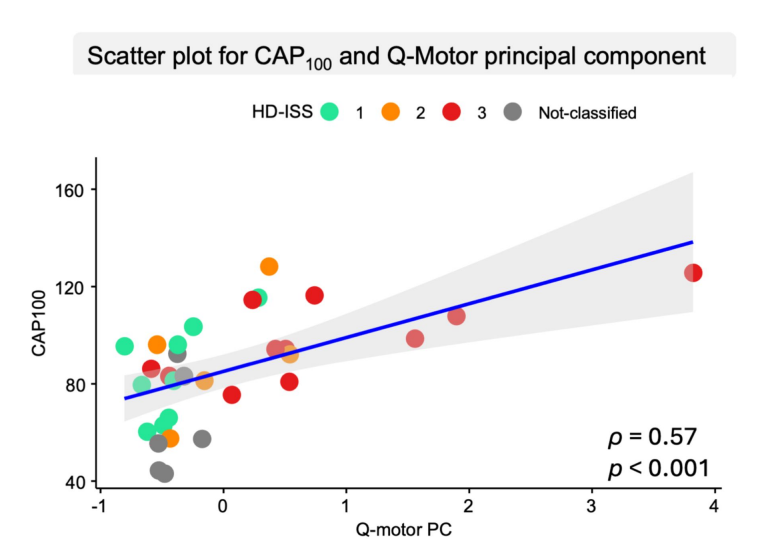


Figure 3. Scatterplot showing positive relationship between the Q-Motor principal component and the disease burden measure (CAP $_{100}$ ) with the Spearman's rho ( $\rho$ ) test.

Rotated Component Loadings on the Q-motor Outcome Measures

Table 5.

Task Task	
Outcome measure	Q-motor Factor
Speeded tapping	
Left finger; Area under the curve (N-s)	0.707
Right finger; Area under the curve (N-s)	0.723
Left finger; Inter-onset interval (s)	0.772
Right finger; Inter-onset interval (s)	0.859
Left foot; Inter-onset interval (s)	0.798
Right foot; Inter-onset interval (s)	0.893
Metronome tapping; Absolute deviation from pace (s)	
Left finger; Paced; Fast	0.875
Left finger; Paced; Slow	0.832
Left finger; Unpaced; Fast	0.936
Left finger; Unpaced; Slow	0.913
Right finger; Paced; Fast	0.730
Right finger; Paced; Slow	0.672
Right finger; Unpaced; Fast	0.886
Right finger; Unpaced; Slow	0.865
Left foot; Paced; Fast	0.823
Left foot; Paced; Slow	0.883
Left foot; Unpaced; Fast	0.884
Left foot; Unpaced; Slow	0.900
Right foot; Paced; Fast	0.818
Right foot; Paced; Slow	0.885
Right foot; Unpaced; Fast	0.890
Right foot; Unpaced; Slow	0.740
Pointing (dominant hand)	
Target frequency over trial (Hz)	-0.525
Pointing (dominant) and tapping (non-dominant)	
Finger tapping area under the curve (N-s)	0.734
Finger tapping inter-onset interval (s)	0.788
Frequency over trial (Hz)	-0.756
Pointing target frequency over trial (Hz)	-0.568

All loadings were significant (>0.5 and < -0.5) and are highlighted in bold.

Abbreviations: Hz: Hertz; N: Newton; s: Seconds

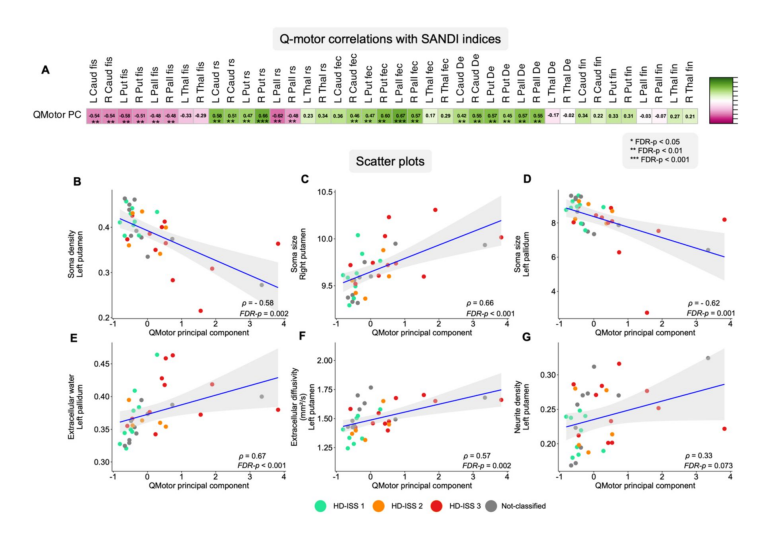


Figure 4.

# A) Correlation matrix and B-G) selected scatter plots illustrating Spearman's rho correlations between SANDI measures and the Q-Motor principal component.

**A)** Each cell represents the Spearman's rho correlation strength, with pink indicating negative and green positive correlations. **B-G)** Each plot includes a best-fit least squares linear regression line with standard error indicated by the grey shaded area, along with the Spearman's rho ( $\rho$ ) and the corresponding FDR-p value. Scatter dot colours represent participants' HD-ISS stage and those who were not classified due to having CAG<40 or incomplete clinical data. **Abbreviations:**  $\mathbf{p}_{e}$ : Extracellular diffusivity;  $\mathbf{f}_{ec}$ : Extracellular signal fraction;  $\mathbf{f}_{in}$ : Neurite density signal fraction;  $\mathbf{f}_{is}$ : Soma density signal fraction;  $\mathbf{PC}$ : Principal component;  $\mathbf{r}_{s}$ : Soma radius; **TFC**: Total functional capacity.

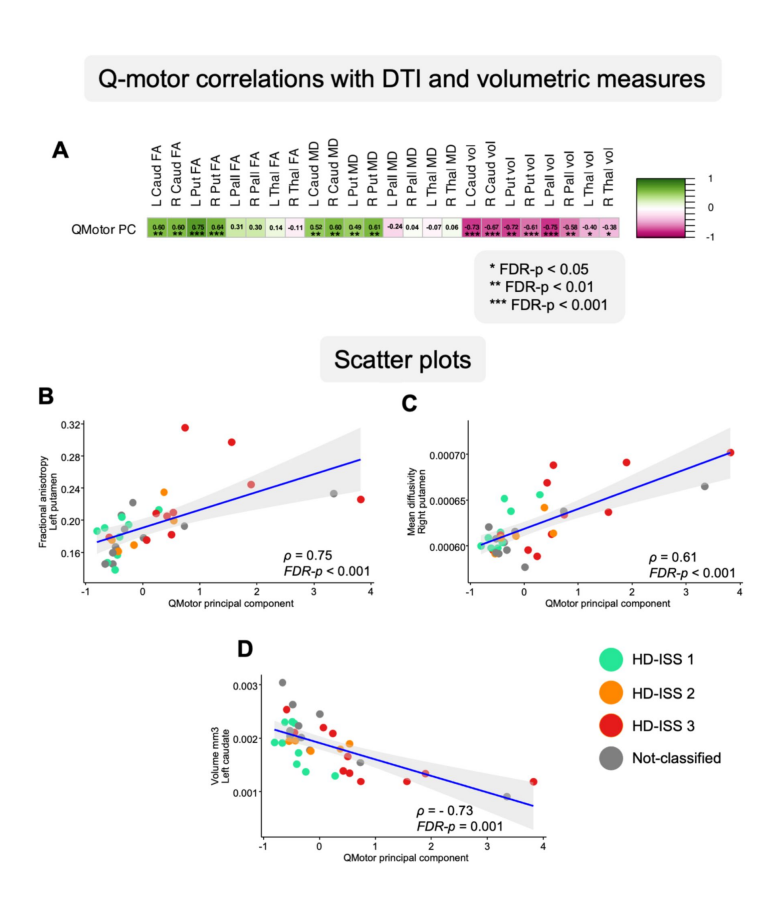


Figure 5.

# A) Correlation matrix and B-D) selected scatter plots illustrating Spearman's rho correlations between DTI, volumetric measures and the Q-Motor principal component.

A) Each cell represents the Spearman's rho correlation strength, with pink indicating negative and green positive correlations. **B-D**) Each plot includes a best-fit least squares linear regression line with standard error indicated by the grey shaded area, along with the Spearman's rho ( $\rho$ ) and the corresponding FDR-p value. Scatter dot colours represent participants' HD-ISS stage and those who were not classified due to having CAG<40 or incomplete clinical data. **Abbreviations: FA**: Fractional anisotropy; **MD**: Mean diffusivity.



# Microstructural predictors of BG volumes

In contrast, regression analyses for the HD data (**Table 7** , **Figures 7** & **8** ) showed that 60% of volume variation in the left caudate and 51% of variation in the right caudate were accounted for by age and apparent soma density and size. Similarly, 57% of variation in the right putamen volume were explained by age and apparent soma size, while 63% of volume differences in the left putamen were explained by age, apparent soma size as well as extracellular signal and diffusivity. Comparable to the healthy control results, age alone accounted for 30% of volume variation in the left and for 35% in the right thalamus while no age effects were present for bilateral globus pallidus. However, in HD patients 42% of volume variation in the left pallidum was explained by apparent soma size and extracellular signal and 27% of volume variation in the right pallidum by extracellular signal fraction only. No significant contributions of TFC were present.

#### Correlation of disease burden with microstructural and volumetric measures

The  ${\rm CAP}_{100}$  score as an index of disease progression was correlated with brain measurements to explore the relationship between disease burden and microstructural and volumetric differences (**Figure 9** ). **Figure 9A** summarises correlation coefficient strengths and levels of significance. **Figures 9B-J** display scatter plots of significant correlations between the  ${\rm CAP}_{100}$  and microstructural and volumetric measures. Increased  ${\rm CAP}_{100}$  was negatively correlated with apparent soma density, and volume size in bilateral caudate and putamen, as well as with pallidal apparent soma size. Positive correlations were observed between  ${\rm CAP}_{100}$  and extracellular diffusivity and signal fraction, apparent soma size in caudate, putamen, and thalamus, apparent neurite density in putamen, FA in the basal ganglia, and MD in caudate and putamen.

# Exploratory pairwise comparisons between HD-ISS premanifest and manifest HD individuals

Compared to the premanifest group, manifest HD individuals exhibited reduced apparent soma density in the striatum, smaller apparent soma size in the pallidum, and increased extracellular diffusivity in the putamen ( $r_{rb}$  = 0.428–0.513, p = 0.01–0.031). Compared to controls, individuals with premanifest HD showed increased extracellular signal fraction in the basal ganglia, larger apparent soma size in the caudate and putamen, and reduced apparent soma density and extracellular diffusivity in the pallidum (rrb = 0.243–0.459, p < 0.001–0.02). The manifest group differed from controls in all measures. Descriptive statistics and statistical analysis results are in Supplementary Table 2. Bar plots displaying effect sizes and 95% confidence intervals for all pairwise comparisons are shown in **Supplementary Figure 1**  $\square$ .

# Figure 6.

# Standardised beta coefficients of SANDI microstructural metrics predicting volume (normalised for intracranial volume) in regions of interest in the healthy control group.

Abbreviations: De: Extracellular diffusivity; fis: Soma density signal fraction; rs: Soma radius; TFC: Total functional capacity. \* *p* < 0.05; \*\* *p* < 0.01; \*\*\* *p* < 0.001.

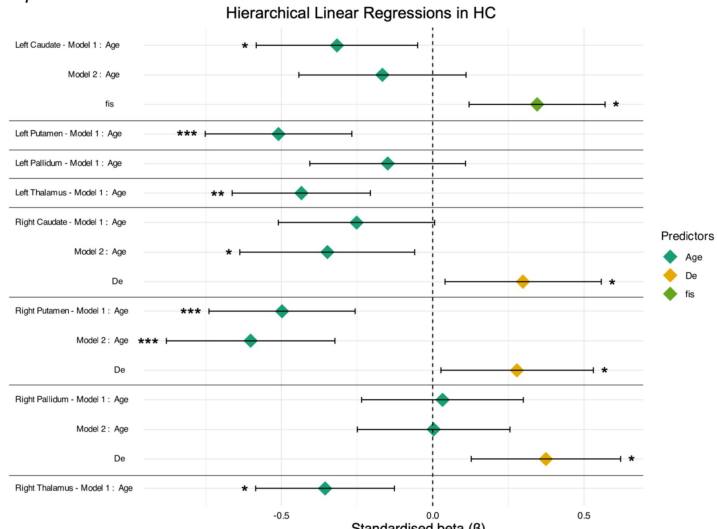


#### Table 6.

# **Hierarchical Linear Regression Predicting Normalised Volumes from SANDI** Microstructural Metrics, Controlling for Age in the Healthy Control Participants

ROI	Model	Predictor(s)	Adjusted R <sup>2</sup>	ΔR²	F-value (p- value)	ΔF-value	в	t-value	p-value
Left Caudate	1	Age	0.084	0.100	6.115 (0.017)		-0.316	-2.473	0.031
	2	Age	0.167	0.096	6.599 (0.003)	6.474	-0.166	-1.226	0.297
		fis					0.345	2.544	0.026
Left Putamen	1	Age	0.247	0.260	19.328 (<0.001)		-0.510	- 4.396	<0.001
Left Pallidum	J	Age	0.004	0.022	1.247 (0.269)		-0.149	-1.117	0.341
Left Thalamus	I I	Age	0.174	0.188	12.761 (0.001)		-0.434	-3.572	0.003
Right Caudate	J.	Age	0.046	0.063	3.715 (0.059)		-0.252	-1.927	0.087
	2	Age	0.111	0.080	4.508 (0.015)	5.029	-0.348	-2.616	0.023
		D <sub>e</sub>					0.299	2.243	0.048
Right Putamen	ı	Age	0.234	0.248	18.109 (<0.001)		-0.498	-4.255	<0.001
	2	Age	0.289	0.067	12.389 (<0.001)	5.265	-0.602	-4.954	< 0.001
		De					0.279	2.295	0.045
Right Pallidum	1	Age	-0.017	0.001	.058 (0.811)		0.032	0.241	0.847
-	2	Age	0.108	0.139	4.392 (0.017)	8.718	0.003	0.025	0.980
		D <sub>e</sub>					0.374	2.953	0.011
Right Thalamus	1	Age	0.111	0.127	7.966 (0.007)		-0.356	-2.822	0.015

Model I: Volume(ROI)= $\beta_0+\beta_1$ \*(Age) + $\epsilon$ ; Model 2-n: Volume (ROI)= $\beta_0+\beta_1$ \*(Age) + $\beta_2$ , $\delta$ \*( $\beta_0$ ,  $\beta_0$ )+ $\delta$ \*( Abbreviations: De: Extracellular diffusivity; fec: Extra TFC: Total Functional Capacity Significant F-values and t-values are highlighted in **bold** 

Table 7.

Hierarchical Linear Regression Models Predicting Normalised Volumes in each Region of Interest from SANDI Microstructural Metrics, Controlling for Age and TFC in HD Gene-Positive Participants

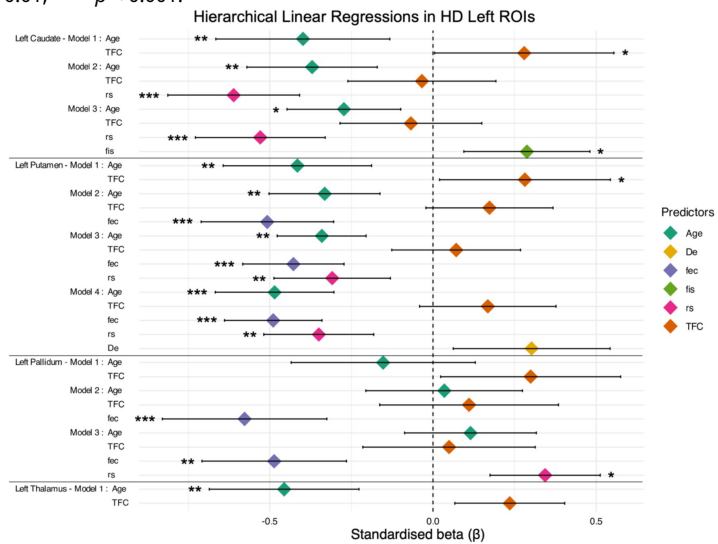
ROI	Model	Predictors	Adjusted R <sup>2</sup>	$\Delta R^2$	F-value (p-value)	ΔF-value	в	t-value	p-value
Left Caudate	1	Age	0.277	0.304	11.136 (<0.001)		-0.398	-3.249	0.005
		TFC					0.280	2.281	0.046
	2	Age	0.547	0.268	22.308 (<0.001)	31.383	-0.370	-3.810	<0.001
		TFC					-0.034	-0.303	0.822
		rs					-0.611	-5.602	<0.001
	3	Age	0.600	0.058	20.853 (<0.001)	7.623	-0.273	-2.788	0.016
		TFC					-0.068	-0.638	0.594
		rs					-0.529	-4.963	<0.001
		fis					0.288	2.761	0.016
Left Putamen	1	Age	0.296	0.323	12.150 (<0.001)		-0.415	-3.436	0.003
		TFC					0.282	2.331	0.043
	2	Age	0.529	0.233	20.855 (<0.001)	26.238	-0.332	-3.311	0.005
		TFC					0.173	1.711	0.129
		fec					-0.507	-5.122	< 0.001
	3	Age	0.601	0.075	20.934 (<0.001)	9.961	-0.341	-3.690	0.003
		TFC					0.071	0.721	0.552
		fec					-0.427	-4.515	<0.001
		r <sub>s</sub>					-0.309	-3.156	0.007
	4	Age	0.630	0.034	19.016 (<0.001)	4.818	-0.485	-4.386	<0.001
		TFC			,,		0.168	1.605	0.157
		fec					-0.489	-5.126	<0.001
		r <sub>s</sub>					-0.349	-3.638	0.003
		D <sub>e</sub>					0.302	2.195	0.052
Left Pallidum	- 1	Age	0.107	0.140	4.165 (0.021)		-0.152	-1.119	0.341
		TFC					0.299	2.198	0.052
	2	Age	0.344	0.241	10.278 (<0.001)	19.485	0.035	0.278	0.829
		TFC					0.111	0.889	0.455
		fec					-0.577	-4.414	<0.001
	3	Age	0.424	0.086	10.741 (<0.001)	7.885	0.115	0.961	0.425
	-	TFC					0.049	0.417	0.753
		fec					-0.486	-3.837	0.001
		rs					0.344	2.808	0.015
Left Thalamus	1	Age	0.302	0.328	12.455 (<0.001)		-0.456	-3.786	0.001
Lete Thatamas		TFC	0.502	0.520	12.133 (30.001)		0.236	1.956	0.085
Right Caudate	ı	Age	0.276	0.304	11.117 (<0.001)		-0.410	-3.341	0.005
rugite Caudate		TFC	0.270	0.501	11.117 (40.001)		0.265	2.162	0.054
	2	Age	0.443	0.171	15.036 (<0.001)	16.233	-0.426	-3.957	0.001
	4	TFC	0.773	0.171	13.030 (~0.001)	10.233	0.006	0.048	0.976
		r <sub>s</sub>					-0.485	-4.029	0.001
	3	Age	0.510	0.073	14.807 (<0.001)	7.898	-0.326	-3.043	0.009
	3	TFC	0.510	0.073	17.007 (~0.001)	7.070	-0.326	-0.156	0.902
							-0.456	-4.020	0.902
		Γs £					0.296	2.810	0.001
Disha Disassa	1	fis	0.222	0.350	14 210 (<0.001)		-0.499		<0.001
Right Putamen	1	Age TFC	0.333	0.358	14.218 (<0.001)		-0.499 0.211	-4.243 1.797	<b>&lt;0.001</b> 0.111
	2		0.570	0.236	24.432 (<0.001)	29.159	-0.425	-4.450	< <b>0.001</b>
	2	Age TFC	0.570	0.236	44.432 (~0.001)	27.137	-0.425	-4.450 -0.652	0.593
							-0.578	-0.652 -5.400	<0.001
D. I. D. II. I		rs	0.042	0.070	2 177 (0 124)				
Right Pallidum	ı	Age	0.043	0.079	2.177 (0.124)		-0.043	-0.308	0.822
	_	TFC					0.264	1.874	0.097
	2	Age	0.265	0.228	7.367 (<0.001)	16.430	0.094	0.737	0.550
		TFC					0.116	0.902	0.454
		fec					-0.530	-4.053	0.001
Right Thalamus	l l	Age	0.347	0.372	15.076 (<0.001)		-0.550	-4.723	<0.001
		TFC					0.145	1.242	0.295

Model I: Volume(ROI)=β<sub>0</sub>+β<sub>1</sub>\*(Age)+β<sub>2</sub>\*(TFC)+ε: Model 2-n: Volume (ROI)=β<sub>0</sub>+β<sub>1</sub>\*(Age)+β<sub>2</sub>\*(TFC)+β<sub>3</sub>-π\*(f<sub>6</sub>, r<sub>6</sub>, f<sub>6</sub>, D<sub>6</sub>, f<sub>6</sub>)+ε: Predictors in Model I were entered simultaneously; predictors in Model 2-n were entered in a stepwise fashion using an iterative forward selection and backward elimination method to maximise the adjusted R³-while keeping only the most significant predictors. Abbreviations: De: Extracellular diffusivity; fec: Extracellular signal Fraction; fin: Neurite density signal fraction; fis: Soma density signal fraction; HD: Huntington's Disease; rs: Soma size; SANDI: Soma And Neurite Density Imaging: TFC. Total Functional Capacity
Significant F-values and t-values (p<0.05) are highlighted in bold

# Figure 7.

Standardised beta coefficients of SANDI microstructural metrics predicting volume (normalised for intracranial volume) in left hemisphere regions of interest in Huntington's disease patients.

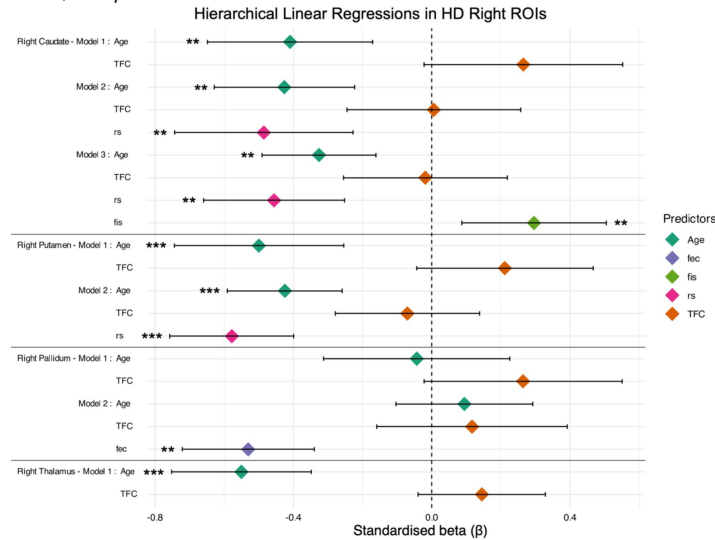
**Abbreviations: De:** Extracellular diffusivity; **fec:** Extracellular signal fraction; **fis:** Soma density signal fraction; **rs:** Soma radius. \* p < 0.05; \*\* p < 0.01; \*\*\* p < 0.001.



# Figure 8.

Standardised beta coefficients of SANDI microstructural metrics predicting volume (normalised for intracranial volume) in right hemisphere regions of interest in Huntington's disease patients.

**Abbreviations: fec:** Extracellular signal fraction; **fis:** Soma density signal fraction; **rs:** Soma radius; **TFC:** Total functional capacity. \* p < 0.05; \*\*\* p < 0.01; \*\*\*\* p < 0.001.



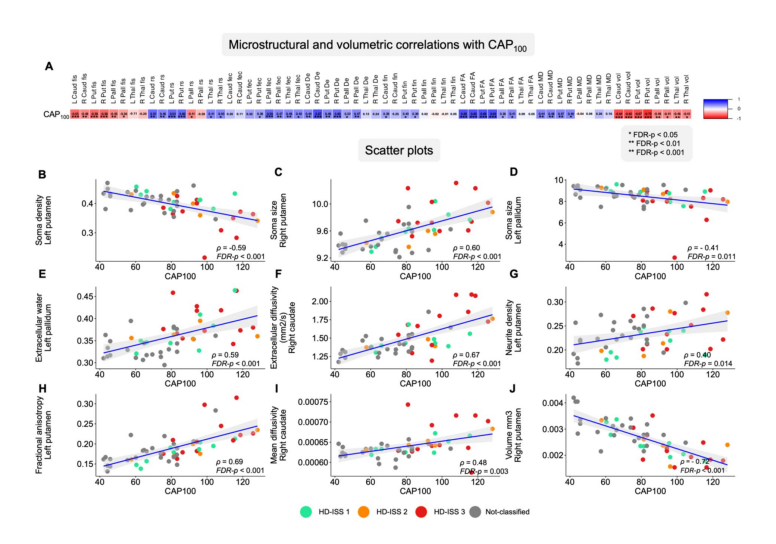


Figure 9.

A) Correlation matrix and **B-J**) selected scatter plots illustrating Spearman's rho correlations between SANDI, DTI, and volumetric measures with CAP100. Each scatter plot includes a best-fit least squares linear regression line with standard error indicated by the grey shaded area, along with the Spearman's rho (ρ) and the corresponding FDR-p value. Scatter dot colours represent participants' HD-ISS stage and those who were not classified due to having CAG < 40 or incomplete clinical data. **Abbreviations: De**: Extracellular diffusivity; **FA**: Fractional anisotropy; **fec**: Extracellular signal fraction; **fin**: Neurite density signal fraction; **fis**: Soma density signal fraction; **MD**: Mean diffusivity; **rs**: Soma radius; **vol**: Normalised volume.



# **Discussion**

This is the first study to investigate HD-related microstructural differences in the basal ganglia with SANDI, a novel diffusion MRI technique, that was devised to probe grey matter microstructure. The objective of the study was to explore SANDI indices as potential non-invasive *in vivo* MRI markers of HD neuropathology that may provide more specific information about disease-related tissue abnormalities than volumetric measurements. SANDI indices of apparent soma density and size were found to be sensitive to HD pathology in the basal ganglia and explained, together with age, up to 63% of striatal atrophy in HD. Furthermore, SANDI indices correlated with motor impairments and CAP100 disease burden in HD. This pattern of results suggests the potential of SANDI indices for future imaging biomarkers of disease progression and of the neural effects of novel disease-modifying therapeutics in HD and other neurodegenerative diseases.

# **Microstructural and Volumetric Alterations in HD**

Well-established patterns of significant volume loss accompanied by increases in FA and MD in the basal ganglia were replicated in HD compared with healthy controls. FA increases in the caudate and putamen are thought to occur due to the selective degeneration of medium spiny neuron connections. No microstructural differences and only trends for volumetric reduction were present in the thalami. This pattern of macro- and microstructural differences in the basal ganglia is in accordance with previously reported changes in the basal ganglia associated with premanifest and early manifest HD stages. 10 cm accordance with previously reported changes in the basal ganglia associated with premanifest and early manifest HD stages.

Importantly, the application of SANDI revealed novel information about HD-related microstructural differences in the basal ganglia. In gene-positive compared with healthy individuals, apparent soma density was reduced and accompanied by increases in extracellular signal fraction and diffusivity across the caudate, putamen, and pallidum but not the thalami. In addition, apparent soma size was increased in the caudate and putamen and reduced in the globus pallidus in individuals with HD.

HD-related reductions of apparent soma density in the basal ganglia are consistent with the loss of striatal medium spiny neurons, the histopathological hallmark of HD, 22 °C, 23 °C and downstream degeneration of pallidal neurons likely due to the loss of striatal projections. Furthermore, changes in apparent soma size may reflect shifts in the proportion of neural and glial cell density and/or changes in cell morphology, including astrocyte and microglia swelling in response to neurodegeneration 22 °C, 24 °C – 26 °C and soma shrinkage prior to neuronal cell death. 86 °C, 87 °C and soma shrinkage prior to neuronal cell death.

Exploratory analyses using stratification into premanifest HD-ISS Stage 1 and manifest Stages 2 and 3 revealed that apparent soma density reductions in the striatum became more pronounced with disease progression. Regional variability of differences in apparent soma size were observed with early increases in the striatum and later reductions in the globus pallidus. Increases in extracellular signal fraction with disease progression were apparent across all basal ganglia ROIs while increases in diffusivity were particularly pronounced in the putamen and pallidum at manifest stages. These preliminary findings suggest that SANDI indices may be sensitive to neuropathological processes associated with different stages of HD.

# Microstructural predictors of basal ganglia atrophy in HD

Regression analyses testing for microstructural predictors of HD-related atrophy in each ROI demonstrated that SANDI indices accounted for a significant proportion of atrophy in the basal ganglia but not the thalami.



Up to 63% of HD-related striatal atrophy was predicted by apparent soma density and size and age. This dropped to 27% and 42% of atrophy in right and left pallidum explained by apparent soma size and extracellular signal fraction, while age alone accounted for volume differences in the thalami. The latter finding in the thalami mirrored the pattern of results in the healthy control data where age was the most significant predictor across all ROIs (except bilateral pallidum) and the only predictor in the thalami, while diffusivity contributed to right-lateralised basal ganglia regions and apparent soma density to left caudate only.

Together these results demonstrate that SANDI indices of apparent soma density and size may capture HD-related differences in striatal grey matter microstructure *in vivo*. As outlined above, striatal reductions in apparent soma density and increases in apparent soma size are in accordance with the HD characteristic loss of medium spiny neurons and reactive gliosis and explained a significant proportion of HD-related atrophy in the caudate and the putamen.

# Associations Between SANDI microstructural indices and Motor Function

The observed correlations between SANDI metrics and motor measures provide novel insights into the functional implications of microstructural alterations in HD. Consistent with the role of the basal ganglia in motor initiation and coordination, the present study demonstrated that microstructural differences in HD, notably reduced apparent soma density in the striatum and reduced apparent soma size in the pallidum were associated with poorer Q-Motor performance, which in turn was associated with larger disease burden. This is evidenced by increased IOI and ACU in speeded tapping tasks, as well as difficulties in the paced metronome tapping task. Similarly, increased apparent soma size in the striatum, as well as elevated extracellular signal and diffusivity across all three basal ganglia regions, and striatal FA and MD, were linked to motor impairments. These findings suggest that microstructural differences due to basal ganglia neurodegeneration and associated glial reactivity are directly linked to subtle motor impairments.

# **Clinical Implications and Future Directions**

The present study acquired multi-shell (max b-value = 6,000 s/mm²) DWI data on a non-clinical ultra-strong gradient (300mT/m) 3T MRI system. Ultra-strong gradient imaging has the advantage of improving the signal-to-noise-ratio at high b-values due to shorter echo times (TE), which in turn provides enhanced sensitivity to small water displacement, 39 cl and minimises bias due to inter-compartmental exchange. 89 cl ,90 cl However, it is important to note that it has been demonstrated feasible to acquire multi-shell DWI data for SANDI modelling on standard clinical 3T MRI systems, 91 cl and that such acquisitions have been shown to be sensitive to neuropathology in MS. 43 cl Thus, it is possible apply SANDI indices clinically.

Our findings highlight the potential of SANDI-derived metrics as future markers for tracking disease progression and assessing therapeutic efficacy in HD and more common neurodegenerative diseases like Alzheimer's and Parkinson's disease. The sensitivity of apparent soma density and size, and extracellular water signal to microstructural changes in HD offers a complementary perspective to volumetric measures, which are currently the most widely employed imaging modality in clinical trials. Furthermore, the associations between SANDI metrics and motor measures that were correlated with disease burden scores underscore their relevance in evaluating the efficacy of emerging disease-modifying treatments.

# Conclusion

In our study, we demonstrate the utility of SANDI for characterising microstructural abnormalities in HD, providing a detailed view of basal ganglia pathology and its implications for motor functions. By bridging the gap between histopathological findings and *in vivo* imaging, SANDI offers a promising avenue for advancing HD research and clinical care.

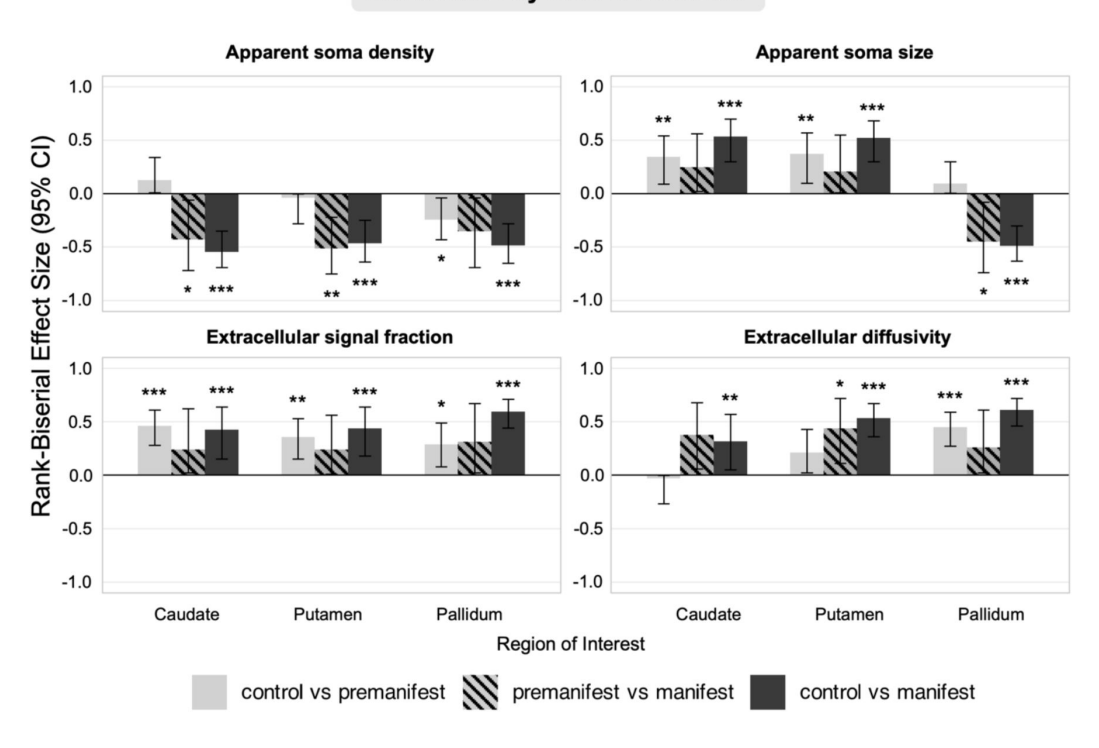


# **Data availability**

This research utilised baseline data from the HD-DRUM project that has been endorsed by the Enroll-HD Scientific Oversight Committee (SOC) (14/11/2022). At the end of the HD-DRUM project, the coded study data will be shared and made accessible to the research community via the Enroll-HD specific data request process.

# **Supplementary figures**

# Effect sizes by SANDI variables



# Supplementary figure 1.

Bar plot showing the effect sizes and 95% confidence intervals for all the exploratory pairwise comparisons between premanifest, manifest and control groups.

Significant comparisons are marked with \* (p < 0.05), \*\* (p < 0.01), and \*\*\* (p < 0.001).



		Stage I		Stage 2		Stage 3		Not-classified
	N	Mean (SD)	N	Mean (SD)	N	Mean (SD)	N	Mean (SD)
Age	9	46.67 (15.14)	5	48.80 (10.83)	12	49.17 (12.20)	30	42.13 (14.28)
Sex, Female (%)	9	6 (66.7%)	5	I (20%)	12	3 (25%)	30	15 (50%)
Education (years)	9	15.67 (1.22	5	14.60 (3.71	12	13.00 (2.17)	12	14.00 (3.13)
MOCA	9	27.56 (1.81)	5	26.00 (2.45)	12	23.73 (3.20)	30	27.23 (3.79)
TOPF	9	50.22 (14.14)	5	44.20 (14.10)	12	43.25 (10.34)	30	53.03 (13.10)
UHDRS-TFC	9	12.89 (0.33)	5	13 (0)	12	10.92 (1.16)	28	12.21 (1.23)
UHDRS-TMS	9	4.00 (4.12)	5	10.2 (1.48)	12	29.33 (20.38)	22	5.64 (10.53)
CAG	9	42 (1.5)	5	42 (I)	12	43.67 (3.14)	24	40.79 (2.57)
CAP <sub>100</sub>	9	84.56 (19.39)	5	91.09 (25.58)	12	99.70 (16.68)	24	67.28 (17.45)
SDMT	9	57.56 (13.17)	5	45.60 (8.73)	12	33.83 (12.65)	12	48.00 (12.62)

Abbreviations: CAG: Cytosine Adenine Guanine; CAP: CAG-Age-Product; HC: Healthy controls; HD: Huntington's disease; HD-ISS: HD-Integrated Staging System; MOCA: Montreal Cognitive Assessment; SD: Standard deviation; SDMT: Symbol Digit Modalities Task; TFC: Total Functional Capacity; TMS: Total Motor Score; TOPF: Test of Premorbid Functioning; UHDRS: United Huntington's Disease Rating Scale

# **Supplementary table 1.**

# Demographic and clinical information per HD-ISS stage.

		Descriptive statistics Mean (SD)			Pairwise comparisons Statistic, (p-value) effect size [CI 95%])				
Microstructural variable	Region of interest	Premanifest N=9	Manifest N=17	Controls N=57	Premanifest vs Controls	Premanifest vs Manifest	Manifest vs Controls		
Apparent soma density	Caudate	0.46 (0.03)	0.41 (0.07)	0.47 (0.02)	311 (0.313) 0.125 [0.01 - 0.35]	117 (0.031) 0.428 [0.08 - 0.71]	850 (<0.001) 0.546 [0.36 - 0.69]		
	Putamen	0.43 (0.03)	0.38 (0.05)	0.43 (0.03)	274 0.75 I 0.04 [0.004 - 0.28]	125 (0.01) 0.513 [0.21 -0.75]	795 (<0.001) 0.464 [0.24 - 0.64]		
	Pallidum	0.21 (0.03)	0.19 (0.03)	0.24 (0.04)	362 (0.05) 0.243 [0.03 - 0.43]	110 (0.075) 0.354 [0.03 - 0.68]	811 (<0.001) 0.488 [0.27 - 0.65]		
Apparent soma size	Caudate	9.73 (0.19)	9.88 (0.28)	9.55 (0.13)	107 (0.005) 0.344 [0.1 - 0.55]	53 (0.215) 0.248 [0.02 - 0.57]	127 (<0.001) 0.534 [0.3 - 0.69]		
	Putamen	9.64 (0.21)	9.77 (0.30)	9.41 (0.14)	94 0.002 0.374 [0.14 - 0.58]	57 (0.306) 0.206 [0.01 - 0.55]	137 (<0.001) 0.519 [0.28 - 0.69]		
	Pallidum	8.89 (0.50)	8.11 (1.44)	8.96 (0.51)	298 0.444 0.095 [0.005 - 0.32]	119 (0.024) 0.449 [0.1 - 0.76]	812 (<0.001) 0.489 [0.29 - 0.64]		
Extracellular signal fraction	Caudate	0.37 (0.01)	0.38 (0.03)	0.36 (0.01)	57 (<0.001) 0.459 [0.28 - 0.59]	54 (0.236) 0.238 [0.01 - 0.6]	200 (<0.001) 0.425 [0.17 - 0.63]		
	Putamen	0.35 (0.01)	0.37 (0.04)	0.33 (0.01)	101 (0.004) 0.358 [0.15 - 0.52]	54 (0.236) 0.238 [0.01 - 0.55]	193 (<0.001) 0.435 [0.17 - 0.65]		
	Pallidum	0.35 (0.04)	0.38 (0.04)	0.33 (0.02)	131 (0.02) 0.289 [0.06 -0.46]	47 (0.118) 0.312 [0.02 - 0.65]	88 (<0.001) 0.592 [0.44 - 0.72]		
Extracellular diffusivity	Caudate	1.42 (0.11)	1.58 (0.24)	1.42 (0.1)	269 (0.823) 0.029 [0.004 - 0.28]	41 (0.059) 0.375 [0.04 - 0.67]	272 (0.006) 0.317 [0.06 – 0.54]		
	Putamen	1.49 (0.11)	1.63 (0.17)	1.43 (0.09)	165 (0.089) 0.21 [0.02 - 0.42]	35 (0.027) 0.439 [0.09 - 0.71]	127 (<0.001) 0.534 [0.37 - 0.67]		
	Pallidum	1.72 (0.17)	1.81 (0.18)	1.53 (0.11)	61 (<0.001) 0.45 [0.28 - 0.59]	52 (0.196) 0.259 [0.01 - 0.62]	76 (<0.001) 0.61 [0.47 - 0.72]		

Abbreviations: CI: Confidence Intervals
Pairwise comparisons were conducted with the Mann-Whitney U tests and reported effect sizes (and 95% CI) represent rank-biserial correlations. Highlighted in bold are significant (p<0.05) tests.

# Supplementary table 2.

Descriptive statistics and non-parametric pairwise comparisons for SANDI indices (significant for HD vs HC) between premanifest, manifest, and control participants.



# **Acknowledgements**

We would like to thank Amy Dangerfield, Allison Cooper and Sonya Foley-Bozorgzad for their help with data collection as well as Derek Jones and John Evans for their advice and support with regards to the implementation of MRI data acquisition protocols. We would like to thank the following clinical and administrative staff at the participating patient identification centres for their help with identifying suitable patients for the study: Eileen Donovan, Kim Munnery, and Jane Davies from the Cardiff HD clinic; Jessica Prado Mota from the Royal Devon University Healthcare NHS Foundation Trust in Exeter; Jenni Burns from the Walton Centre NHS Foundation Trust in Liverpool; Natalie Rosewell, Anya Soonderpershad, and Dr Liz Coulthard from the Bristol Brain Centre; Claire Tilley and Dr Hugh Rickards from the Birmingham and Solihull Mental Health NHS Foundation Trust. In addition, we would like to thank all Public Involvement contributors and the members of the Enroll-HD Scientific Oversight Committee for their input into the study as well as all participants for their generous time commitment to help us conducting this research.

# **Additional information**

# **Funding**

This work was supported by a National Institute for Health Research (NIHR) and Health and Care Research Wales (HCRW) Advanced Fellowship to CM-B (grant number: NIHR-FS(A)-2022). The Centre for Trials Research at Cardiff University receives infrastructure funding from HCRW. MP is supported by the UKRI Future Leaders Fellowship MR/T020296/2. CC was funded by a Wellcome Trust PhD studentship (204005/Z/16/Z) and LL by a PhD studentship of the School of Psychology at Cardiff University. The WANDI project was funded by a Wellcome Trust Investigator Award (096646/Z/11/Z), a Wellcome Trust Strategic Award (104943/Z/14/Z), and a Wellcome Discovery Awards (227882/Z/23/Z and 317797/Z/24/Z).

# **Funding**

National Institute for Health Research (NIHR-FS(A)-2022)

• Claudia Metzler-Baddeley

Health and Care Research Wales (NIHR-FS(A)-2022)

• Claudia Metzler-Baddeley

UKRI (MR/T020296/2)

• Marco Palombo

**Wellcome Trust** 

https://doi.org/10.35802/204005 🚅

Chiara Casella



# **Cardiff University**

• Lucy Layland

# Wellcome Trust

https://doi.org/10.35802/096646 🔁

# Wellcome Trust

https://doi.org/10.35802/227882 🗗

**Wellcome Trust (317797/Z/24/Z)** 

# Wellcome Trust

https://doi.org/10.35802/104943 🔁



# References

- 1. Rüb U, Seidel K, Heinsen H, Vonsattel JP, den Dunnen WF, Korf HW. (2016) **Huntington's disease (HD): the neuropathology of a multisystem neurodegenerative disorder of the human brain** *Brain Pathology* **26**:726–740 https://doi.org/10.1111/bpa.12426 | Google Scholar
- Tabrizi SJ, Scahill RI, Durr A, et al. (2011) Biological and clinical changes in premanifest and early stage Huntington's disease in the TRACK-HD study: the 12-month longitudinal analysis Lancet Neurol 10:31–42 https://doi.org/10.1016/S1474-4422(10)70276-3 | Google Scholar
- 3. Roos RAC (2010) **Huntington's disease: A clinical review** *Orphanet J Rare Dis* **5** https://doi.org/10.1186/1750-1172-5-40 | Google Scholar
- 4. Walker FO. (2007) **Huntington's disease** *The Lancet* **369**:218–228 https://doi.org/10.1016 /S0140-6736(07)60111-1 | Google Scholar
- Ross CA, Aylward EH, Wild EJ, et al. (2014) Huntington disease: Natural history, biomarkers and prospects for therapeutics Nat Rev Neurol 10:204–216 https://doi.org/10.1038/nrneurol .2014.24 | Google Scholar
- Aylward EH, Liu D, Nopoulos PC, et al. (2012) Striatal volume contributes to the prediction of onset of Huntington disease in incident cases Biol Psychiatry 71:822–828 https://doi.org/10 .1016/j.biopsych.2011.07.030 | Google Scholar
- 7. Tan B, Shishegar R, Poudel GR, Fornito A, Georgiou-Karistianis N (2021) **Cortical morphometry and neural dysfunction in Huntington's disease: a review** *Eur J Neurol* **28**:1406–1419 https: //doi.org/10.1111/ene.14648 | Google Scholar
- 8. Kinnunen KM, Schwarz AJ, Turner EC, et al. (2021) Volumetric MRI-Based Biomarkers in Huntington's Disease: An Evidentiary Review Front Neurol 12 https://doi.org/10.3389/fneur.2021.712555 | Google Scholar
- Wilkes FA, Abaryan Z, Ching CRK, et al. (2019) Striatal morphology and neurocognitive dysfunction in Huntington disease: The IMAGE-HD study Psychiatry Res Neuroimaging 291:1– 8 https://doi.org/10.1016/j.pscychresns.2019.07.003 | Google Scholar
- Scahill RI, Zeun P, Osborne-Crowley K, et al. (2020) Biological and Clinical Characteristics of Gene Carriers Far from Predicted Onset in the Huntington's Disease Young Adult Study (HD-YAS): A Cross-Sectional Analysis Lancet Neurol 19:502–512 Google Scholar
- 11. Paulsen JS, Langbehn DR, Stout JC, et al. (2008) **Detection of Huntington's disease decades before diagnosis: The Predict-HD study** *J Neurol Neurosurg Psychiatry* **79**:874–880 https://doi
  org/10.1136/jnnp.2007.128728 | Google Scholar
- 12. Biglan KM, Zhang Y, Long JD, et al. (2013) **Refining the diagnosis of huntington disease: The PREDICT-HD study** *Front Aging Neurosci* **5**:1–8 https://doi.org/10.3389/fnagi.2013.00012 | Google Scholar



- 13. Tabrizi SJ, Langbehn DR, Leavitt BR, et al. (2009) Biological and clinical manifestations of Huntington's disease in the longitudinal TRACK-HD study: cross-sectional analysis of baseline data Lancet Neurol 8:791–801 https://doi.org/10.1016/S1474-4422(09)70170-X | Google Scholar
- 14. Tabrizi SJ, Reilmann R, Roos RA, et al. (2012) Potential endpoints for clinical trials in premanifest and early Huntington's disease in the TRACK-HD study: analysis of 24 month observational data Lancet Neurol 11:42–53 https://doi.org/10.1016/S1474-4422(11)70263-0 | Google Scholar
- Tabrizi SJ, Scahill RI, Owen G, et al. (2013) Predictors of phenotypic progression and disease onset in premanifest and early-stage Huntington's disease in the TRACK-HD study: Analysis of 36-month observational data Lancet Neurol 12:637–649 https://doi.org/10.1016/ /S1474-4422(13)70088-7 | Google Scholar
- 16. Tabrizi SJ, Estevez-Fraga C, van Roon-Mom WMC, et al. (2022) Potential disease-modifying therapies for Huntington's disease: lessons learned and future opportunities Lancet Neurol 21:645–658 https://doi.org/10.1016/S1474-4422(22)00121-1 | Google Scholar
- 17. Vonsattel PJG, Keller C, Cortes Ramirez PE. (2011) **Huntington's disease-neuropathology** *Handbook of Clinical Neurology* **100**:83–100 Google Scholar
- Liu CF, Younes L, Tong X, et al. (2023) Longitudinal imaging highlights preferential basal ganglia circuit atrophy in Huntington's disease Brain Commun 5 https://doi.org/10.1093 /braincomms/fcad214 | Google Scholar
- 19. Johnson EB, Ziegler G, Penny W, et al. (2021) **Dynamics of Cortical Degeneration Over a Decade in Huntington's Disease** *Biol Psychiatry* **89**:807–816 https://doi.org/10.1016/j

  .biopsych.2020.11.009 | Google Scholar
- 20. Estevez-Fraga C, Scahill R, Rees G, Tabrizi SJ, Gregory S (2021) **Diffusion imaging in Huntington's disease: Comprehensive review** *J Neurol Neurosurg Psychiatry* **92**:62–69 https://doi.org/10.1136/jnnp-2020-324377 | Google Scholar
- 21. Tabrizi SJ, Schobel S, Gantman EC, et al. (2022) A biological classification of Huntington's disease: the Integrated Staging System Lancet Neurol 21:632–644 https://doi.org/10.1016/S1474-4422(22)00120-X | Google Scholar
- Myers RH, Vonsattel JP, Paskevich PA, et al. (1991) Decreased Neuronal and Increased Oligodendroglial Densities in Huntington's Disease Caudate Nucleus J Neuropathol Exp Neurol 50:729-742 https://doi.org/10.1097/00005072-199111000-00005 | Google Scholar
- 23. Vis JC, Schipper E, de Boer-van H, et al. (2005) Expression pattern of apoptosis-related markers in Huntington's disease Acta Neuropathol 109:321–328 https://doi.org/10.1007/s00401-004-0957-5 | Google Scholar
- Vis JC, Nicholson LFB, Faull RLM, Evans WH, Severs NJ, Green CR (1998) Connexin expression in Huntington's diseased human brain Cell Biol Int 22:837–847 https://doi.org/10.1006/cbir .1998.0388 | Google Scholar



- Simmons DA, Casale M, Alcon B, Pham N, Narayan N, Lynch G (2007) Ferritin accumulation in dystrophic microglia is an early event in the development of Huntington's Disease Glia 55:1074–1084 https://doi.org/10.1002/glia.20526 | Google Scholar
- 26. Sapp E, Kegel KB, Aronin N, et al. (2001) Early and Progressive Accumulation of Reactive Microglia in the Huntington Disease Brain J Neuropathol Exp Neurol 60:161–172 https://doi.org/10.1093/jnen/60.2.161 | Google Scholar
- 27. Le Bihan D, Turner R, Moonen CTW, Pekar J (1991) **Imaging of diffusion and microcirculation** with gradient sensitization: Design, strategy, and significance Journal of Magnetic Resonance Imaging 1:7–28 https://doi.org/10.1002/jmri.1880010103 | Google Scholar
- 28. Basser PJ, Mattiello J, LeBihan D (1994) MR diffusion tensor spectroscopy and imaging Biophys J 66:259–267 https://doi.org/10.1016/S0006-3495(94)80775-1 | Google Scholar
- Basser PJ, Pierpaoli C (1996) Microstructural and Physiological Features of Tissues
   Elucidated by Quantitative-Diffusion-Tensor MRI J Magn Reson B 111:209–219 https://doi.org/10.1006/jmrb.1996.0086 | Google Scholar
- Georgiou-Karistianis N, Gray MA, Domínguez D JF, et al. (2013) Automated differentiation of pre-diagnosis Huntington's disease from healthy control individuals based on quadratic discriminant analysis of the basal ganglia: The IMAGE-HD study Neurobiol Dis 51:82– 92 https://doi.org/10.1016/j.nbd.2012.10.001 | Google Scholar
- 31. Hobbs NZ, Cole JH, Farmer RE, et al. (2013) Evaluation of multi-modal, multi-site neuroimaging measures in Huntington's disease: Baseline results from the PADDINGTON study Neuroimage Clin 2:204–211 https://doi.org/10.1016/j.nicl.2012.12.001 | Google Scholar
- 32. Jones DK, Alexander DC, Bowtell R, et al. (2018) Microstructural imaging of the human brain with a 'super-scanner': 10 key advantages of ultra-strong gradients for diffusion MRI Neuroimage 182:8–38 https://doi.org/10.1016/j.neuroimage.2018.05.047 | Google Scholar
- 33. Assaf Y, Basser PJ (2005) Composite hindered and restricted model of diffusion (CHARMED) MR imaging of the human brain Neuroimage 27:48–58 https://doi.org/10.1016/j.neuroimage .2005.03.042 | Google Scholar
- Zhang H, Schneider T, Wheeler-Kingshott CA, Alexander DC (2012) NODDI: Practical in vivo neurite orientation dispersion and density imaging of the human brain Neuroimage
   61:1000–1016 https://doi.org/10.1016/j.neuroimage.2012.03.072 | Google Scholar
- Martinez-Heras E, Grussu F, Prados F, Solana E, Llufriu S (2021) Diffusion-Weighted Imaging: Recent Advances and Applications. Seminars in Ultrasound CT and MRI 42:490–506 https://doi.org/10.1053/j.sult.2021.07.006 | Google Scholar
- Daducci A, Dal Palu A, Lemkaddem A, Thiran JP (2015) COMMIT: Convex Optimization Modeling for Microstructure Informed Tractography IEEE Trans Med Imaging 34:246– 257 https://doi.org/10.1109/TMI.2014.2352414 | Google Scholar
- 37. Zhang J, Gregory S, Scahill RI, et al. (2018) In vivo characterization of white matter pathology in premanifest huntington's disease *Ann Neurol* **84**:497–504 https://doi.org/10.1002/ana.25309 | Google Scholar
- Palombo M, Ianus A, Guerreri M, et al. (2020) SANDI: A compartment-based model for noninvasive apparent soma and neurite imaging by diffusion MRI Neuroimage



- 215:116835 https://doi.org/10.1016/j.neuroimage.2020.116835 | Google Scholar
- 39. Koller K, Rudrapatna U, Chamberland M, et al. (2021) MICRA: Microstructural image compilation with repeated acquisitions Neuroimage 225:117406 https://doi.org/10.1016/j.neuroimage.2020.117406 | Google Scholar
- 40. Ianuş A, Carvalho J, Fernandes FF, et al. (2022) Soma and Neurite Density MRI (SANDI) of the in-vivo mouse brain and comparison with the Allen Brain Atlas Neuroimage 254 https://doi.org/10.1016/j.neuroimage.2022.119135 | Google Scholar
- Krijnen EA, Russo AW, Salim Karam E, et al. (2023) Detection of grey matter microstructural substrates of neurodegeneration in multiple sclerosis Brain Commun 5 https://doi.org/10 .1093/braincomms/fcad153 | Google Scholar
- 42. Margoni M, Pagani E, Preziosa P, et al. (2023) **In vivo quantification of brain soma and neurite density abnormalities in multiple sclerosis** *J Neurol* **270**:433–445 https://doi.org/10.1007/s00415-022-11386-3 | Google Scholar
- 43. Barakovic M, Weigel M, Cagol A, et al. (2024) A novel imaging marker of cortical "cellularity" in multiple sclerosis patients Sci Rep 14:9848 https://doi.org/10.1038/s41598-024-60497-6 | Google Scholar
- 44. Byrne LM, Rodrigues FB, Johnson EB, et al. (2018) **Evaluation of Mutant Huntingtin and Neurofilament Proteins as Potential Markers in Huntington's Disease 10** https://www.science.org
- 45. Sampedro F, Pérez-Pérez J, Martínez-Horta S, et al. (2021) Cortical microstructural correlates of plasma neurofilament light chain in Huntington's disease Parkinsonism Relat Disord 85:91–94 https://doi.org/10.1016/j.parkreldis.2021.03.008 | Google Scholar
- 46. Bechtel N, Scahill RI, Rosas HD, et al. (2010) **Tapping linked to function and structure in premanifest and symptomatic Huntington disease** *Neurology* **75**:2150–2160 https://doi.org/10.1212/WNL.0b013e3182020123 | Google Scholar
- 47. Warner JH, Long JD, Mills JA, et al. (2022) Standardizing the CAP Score in Huntington's Disease by Predicting Age-at-Onset J Huntingtons Dis 11:153–171 https://doi.org/10.3233/JHD -210475 | Google Scholar
- 48. Ioakeimidis V, Busse M, Drew CJG, et al. (2024) Protocol for a randomised controlled unblinded feasibility trial of HD-DRUM: a rhythmic movement training application for cognitive and motor symptoms in people with Huntington's disease BMJ Open 14:e082161 https://doi.org/10.1136/bmjopen-2023-082161 | Google Scholar
- Casella C, Chamberland M, Laguna PL, et al. (2022) Mutation-related magnetization-transfer, not axon density, drives white matter differences in premanifest Huntington disease: Evidence from in vivo ultra-strong gradient MRI Hum Brain Mapp: 3439–3460 https://doi.org/10.1002/hbm.25859 | Google Scholar
- McNabb CB, Driver ID, Hyde V, et al. (2025) WAND: A multi-modal dataset integrating advanced MRI, MEG, and TMS for multi-scale brain analysis Sci Data 12:220 https://doi.org /10.1038/s41597-024-04154-7 | Google Scholar
- 51. Siesling S, Van Vugt JPP, Zwinderman KAH, Kieburtz K, Roos RAC (1998) **Unified Huntington's**disease rating scale: A follow up Movement Disorders **13**:915–919 https://doi.org/10.1002



### /mds.870130609 | Google Scholar

- 52. Nasreddine ZS, Phillips NA, Bédirian V, et al. (2005) **The Montreal Cognitive Assessment, MoCA: A Brief Screening Tool For Mild Cognitive Impairment** *J Am Geriatr Soc* **53**:695–699 https://doi.org/10.1111/j.1532-5415.2005.53221.x | Google Scholar
- 53. Wechsler D (2011) Test of Premorbid Functioning Google Scholar
- 54. Anonymous (1996) **Unified Huntington's disease rating scale: Reliability and consistency** *Movement Disorders.* **11**:136–142 https://doi.org/10.1002/mds.870110204 | Google Scholar
- 55. Smith A. (1973) Symbol Digit Modalities Test (SDMT) WPS Google Scholar
- 56. Schubert R, Fiedler H, Barallon P, Habbel B, Reilmann R (2022) **F55 Q-motor speeded tapping** and pointing assessments: feasibility of a dual task design. In: F: Clinical Studies: Case Reports Observational Studies and Trials: A56.1–A56 https://doi.org/10.1136/jnnp-2022-ehdn .146 | Google Scholar
- 57. Schubert R, Rosser A, Bachoud-Lévi AC, Craufurd D, Reilmann R (2018) **F63 Preliminary results from Q-MOTOR/Q-COG analyses in the repair-hd study** *Clinical Studies* :A62.1–A62 https://doi.org/10.1136/jnnp-2018-EHDN.164 | Google Scholar
- 58. Reilmann R, Schubert R (2017) Motor Outcome Measures in Huntington Disease Clinical Trials Elsevier B.V. https://doi.org/10.1016/B978-0-12-801893-4.00018-3 | Google Scholar
- 59. Reilmann R, Rosser A, Kostyk S, et al. (2021) F41 The proof-hd phase 3 study: pridopidine's outcome on function in huntington disease (PROOF) F: Clinical Studies: Case Reports, Observational Studies and Trials BMJ Publishing Group Ltd: A36.1–A36 https://doi.org/10.1136/jnnp-2021-EHDN.84 | Google Scholar
- Reilmann R, Anderson KE, Feigin A, et al. (2024) Safety and efficacy of laquinimod for Huntington's disease (LEGATO-HD): a multicentre, randomised, double-blind, placebocontrolled, phase 2 study Lancet Neurol 23:243–255 https://doi.org/10.1016/S1474 -4422(23)00454-4 | Google Scholar
- Hermle D, Schubert R, Barallon P, et al. (2024) Multifeature quantitative motor assessment of upper limb ataxia including drawing and reaching Ann Clin Transl Neurol 11:1097– 1109 https://doi.org/10.1002/acn3.52024 | Google Scholar
- 62. Tuch DS, Reese TG, Wiegell MR, Makris N, Belliveau JW, Wedeen VJ (2002) **High angular** resolution diffusion imaging reveals intravoxel white matter fiber heterogeneity Magn Reson Med **48**:577–582 https://doi.org/10.1002/mrm.10268 | Google Scholar
- 63. Smith SM (2002) Fast robust automated brain extraction Hum Brain Mapp 17:143–155 https://doi.org/10.1002/hbm.10062 | Google Scholar
- 64. Tournier JD, Smith R, Raffelt D, et al. (2019) MRtrix3: A fast, flexible and open software framework for medical image processing and visualisation Neuroimage 202 https://doi.org/10.1016/j.neuroimage.2019.116137 | Google Scholar
- Leemans A, Jeurissen B, Sijbers J, Jones DK. (2009) **ExploreDTI: a graphical toolbox for processing, analyzing, and visualizing diffusion MR data** In: *ISMRM* Google Scholar



- 66. Sairanen V, Leemans A, Tax CMW (2018) Fast and accurate Slicewise OutLIer Detection (SOLID) with informed model estimation for diffusion MRI data Neuroimage 181:331–346 https://doi.org/10.1016/j.neuroimage.2018.07.003 | Google Scholar
- Andersson JLR, Skare S, Ashburner J (2003) How to correct susceptibility distortions in spinecho echo-planar images: application to diffusion tensor imaging Neuroimage 20:870– 888 https://doi.org/10.1016/S1053-8119(03)00336-7 | Google Scholar
- Smith SM, Jenkinson M, Woolrich MW, et al. (2004) Advances in functional and structural MR image analysis and implementation as FSL Neuroimage 23:S208–S219 https://doi.org/10.1016/j.neuroimage.2004.07.051 | Google Scholar
- Andersson JLR, Sotiropoulos SN (2016) An integrated approach to correction for offresonance effects and subject movement in diffusion MR imaging Neuroimage 125:1063– 1078 https://doi.org/10.1016/j.neuroimage.2015.10.019 | Google Scholar
- Kellner E, Dhital B, Kiselev VG, Reisert M (2016) Gibbs-ringing artifact removal based on local subvoxel-shifts Magn Reson Med 76:1574–1581 https://doi.org/10.1002/mrm.26054 | Google Scholar
- 71. Cordero-Grande L, Christiaens D, Hutter J, Price AN, Hajnal J V (2019) Complex diffusion-weighted image estimation via matrix recovery under general noise models Neuroimage 200:391–404 https://doi.org/10.1016/j.neuroimage.2019.06.039 | Google Scholar
- 72. Veraart J, Fieremans E, Novikov DS (2016) **Diffusion MRI noise mapping using random matrix theory** *Magn Reson Med* **76**:1582–1593 https://doi.org/10.1002/mrm.26059 | Google Scholar
- 73. Veraart J, Novikov DS, Christiaens D, Ades-aron B, Sijbers J, Fieremans E (2016) **Denoising of diffusion MRI using random matrix theory** *Neuroimage* **142**:394–406 https://doi.org/10.1016/j.neuroimage.2016.08.016 | Google Scholar
- 74. Fischl B. (2012) FreeSurfer Neuroimage 62:774–781 https://doi.org/10.1016/j.neuroimage.2012 .01.021 | Google Scholar
- Jenkinson M (2002) Improved Optimization for the Robust and Accurate Linear
   Registration and Motion Correction of Brain Images Neuroimage 17:825–841 https://doi.org/10.1016/S1053-8119(02)91132-8 | Google Scholar
- 76. JASP Team (2023) **JASP**
- 77. R Core Team (2024) R: A Language and Environment for Statistical Computing
- 78. RStudio Team (2024) RStudio: Integrated Development for R
- 79. IBM Corp (2024) **IBM SPSS Statistics for Windows** Google Scholar
- 80. Benjamini Y, Hochberg Y (1995) Controlling the False Discovery Rate: A Practical and Powerful Approach to Multiple Testing J R Stat Soc Series B Stat Methodol 57:289–300 https://doi.org/10.1111/j.2517-6161.1995.tb02031.x | Google Scholar



- 81. Lakens D (2014) **Performing high-powered studies efficiently with sequential analyses** *Eur J Soc Psychol* **44**:701–710 https://doi.org/10.1002/ejsp.2023 | Google Scholar
- 82. Preacher KJ, MacCallum RC (2002) Exploratory Factor Analysis in Behavior Genetics
  Research: Factor Recovery with Small Sample Sizes Behav Genet 32:153–161 https://doi.org/10.1023/A:1015210025234 | Google Scholar
- 83. de Winter JCF, Dodou D, Wieringa PA (2009) Exploratory Factor Analysis With Small Sample Sizes Multivariate Behav Res 44:147–181 https://doi.org/10.1080/00273170902794206 | Google Scholar
- 84. Matz OC, Spocter M (2022) The Effect of Huntington's Disease on the Basal Nuclei: A Review Cureus https://doi.org/10.7759/cureus.24473 | Google Scholar
- 85. Sánchez-Castañeda C, Cherubini A, Elifani F, et al. (2013) **Seeking huntington disease** biomarkers by multimodal, cross-sectional basal ganglia imaging *Hum Brain Mapp* **34**:1625–1635 https://doi.org/10.1002/hbm.22019 | Google Scholar
- 86. Fricker M, Tolkovsky AM, Borutaite V, Coleman M, Brown GC. (2018) **Neuronal Cell Death**Physiol Rev. **98**:813–880 https://doi.org/10.1152/physrev.00011.2017 | Google Scholar
- 87. Kerr JFR, Wyllie AH, Currie AR (1972) **Apoptosis: A Basic Biological Phenomenon with Wideranging Implications in Tissue Kinetics** *Br J Cancer* **26**:239–257 https://doi.org/10.1038/bjc.1972.33 | Google Scholar
- 88. Klaus A, Alves da Silva J, Costa RM. (2019) What, If, and When to Move: Basal Ganglia Circuits and Self-Paced Action Initiation Annu Rev Neurosci 42:459–483 https://doi.org/10.1146/annurev-neuro-072116-031033 | Google Scholar
- 89. Olesen JL, Østergaard L, Shemesh N, Jespersen SN (2022) **Diffusion time dependence, power-law scaling, and exchange in gray matter** *Neuroimage* **251**:118976 https://doi.org/10.1016/j.neuroimage.2022.118976 | Google Scholar
- 90. Jelescu IO, de Skowronski A, Geffroy F, Palombo M, Novikov DS (2022) Neurite Exchange Imaging ((NEXI): A minimal model of diffusion in gray matter with inter-compartment water exchange Neuroimage 256 https://doi.org/10.1016/j.neuroimage.2022.119277 | Google Scholar
- 91. Schiavi S, Palombo M, Zacà D, et al. (2023) Mapping tissue microstructure across the human brain on a clinical scanner with soma and neurite density image metrics Hum Brain Mapp 44:4792–4811 https://doi.org/10.1002/hbm.26416 | Google Scholar

# **Author information**

### **Vasileios Ioakeimidis**

Cardiff University Brain Research Imaging Centre (CUBRIC), School of Psychology, Cardiff University, Cardiff, United Kingdom, Danish Research Centre for Magnetic Resonance, Department for Radiology and Nuclear Medicine, Copenhagen University Hospital Amager and Hvidovre, Copenhagen, Denmark



#### Marco Palombo

Cardiff University Brain Research Imaging Centre (CUBRIC), School of Psychology, Cardiff University, Cardiff, United Kingdom

#### Chiara Casella

Department for Forensic and Neurodevelopmental Sciences, Institute of Psychiatry, Psychology and Neuroscience, King's College London, London, United Kingdom, Early life imaging research department, School of Biomedical Engineering and Imaging Sciences, King's College London, London, United Kingdom, London Collaborative Ultra high field System (LoCUS), Kings College London, London, United Kingdom ORCID iD: 0000-0002-0292-3330

### **Lucy Layland**

Cardiff University Brain Research Imaging Centre (CUBRIC), School of Psychology, Cardiff University, Cardiff, United Kingdom

# Carolyn B McNabb

Cardiff University Brain Research Imaging Centre (CUBRIC), School of Psychology, Cardiff University, Cardiff, United Kingdom

#### **Robin Schubert**

George Huntington Institut (GHI), Münster, Germany

# **Philip Pallmann**

Centre for Trials Research, School of Medicine, Cardiff University, Cardiff, United Kingdom

#### **Monica E Busse**

Centre for Trials Research, School of Medicine, Cardiff University, Cardiff, United Kingdom

#### Cheney JG Drew

Centre for Trials Research, School of Medicine, Cardiff University, Cardiff, United Kingdom

#### **Sundus Alusi**

The Walton Centre for Neurology and Neurosurgery, Liverpool, United Kingdom

# **Timothy Harrower**

Royal Devon and Exeter NHS Trust, Exeter, United Kingdom

#### **Anne E Rosser**

Cardiff University Brain Repair Group, School of Biosciences, Cardiff University, Cardiff, United Kingdom, Advanced Neurotherapeutics Centre (ANTC), Department of Neurology and Psychological Medicine, School of Medicine, Cardiff University, Cardiff, United Kingdom ORCID iD: 0000-0002-4716-4753

#### **Claudia Metzler-Baddeley**

Cardiff University Brain Research Imaging Centre (CUBRIC), School of Psychology, Cardiff University, Cardiff, United Kingdom

ORCID iD: 0000-0002-8646-1144

For correspondence: metzler-baddeleyc@cardiff.ac.uk



### **Editors**

**Reviewing Editor** 

#### Jason Lerch

University of Oxford, Oxford, United Kingdom

Senior Editor

#### **Tamar Makin**

University of Cambridge, Cambridge, United Kingdom

#### Reviewer #1 (Public review):

- (1) In this study, the authors aimed at characterizing Huntington's Disease (HD) related microstructural abnormalities in the basal ganglia and thalami as revealed using Soma and Neurite Density Imaging (SANDI) indices (apparent soma density, apparent soma size, extracellular water signal fraction, extracellular diffusivity, apparent neurite density, fractional anisotropy and mean diffusivity).
- (2) The study implements a novel biophysical diffusion model that extends up-to-date methodologies and presents a significant potential for quantifying neurodegenerative processes of the grey matter of the human brain in vivo. The authors comment on the usefulness of this technique in other pathologies, but they exemplify it only with multiple sclerosis. Further development of this, building evidence, should be provided.
- (3) The study found that HD-related neurodegeneration in the striatum accounted significantly for striatal atrophy and correlated with motor impairments. HD was associated with reduced soma density, increased apparent soma size, and extracellular signal fraction in the basal ganglia, but not in the thalami. Additionally, these effects were larger at the manifest stage.
- (4) The results of this work demonstrate the impact of HD on the basal ganglia and thalami, which can be further explored as a non-invasive biomarker of disease progression. Additionally, the study shows that SANDI can be used to explore grey matter microstructure in a variety of neurological conditions.

https://doi.org/10.7554/eLife.107661.1.sa3

### Reviewer #2 (Public review):

# Summary:

The authors aimed to investigate whether advanced microstructural diffusion MRI modeling using the SANDI framework could reveal clinically relevant tissue alterations in the subcortical structures of individuals with Huntington's disease (HD). Specifically, they sought to determine if SANDI-derived parameters-such as soma density, soma size, and extracellular diffusivity-could detect abnormalities in both manifest and premanifest HD stages, complement standard MRI biomarkers (e.g., volume, MD), and correlate with disease burden and motor impairment. Through this, they hoped to demonstrate the feasibility and added biological specificity of SANDI for early detection and characterization of HD pathology.

# Strengths:

(1) Novelty and relevance:



This is, to the best of my knowledge, the first clinical deployment of SANDI in HD, offering more biophysically interpretable and specific imaging biomarkers than standard DTI or volumetric features.

- (2) More specific microstructural insight: Traditional approaches have used volumetric features (e.g., striatal volume loss) or DTI metrics (like FA and MD), which are indirect and non-specific markers. They can indicate something is "wrong" but not what is wrong.
- (3) SANDI parameters permit establishing clearer links with microstructure:
- o Apparent soma density (fis): proxy for neuronal/glial cell body density.
- o Apparent soma size (rs): reflects possible gliagl hypertrophy or neuronal shrinkage.
- o Neurite density (fin): linked to dendritic/axonal integrity.
- o Extracellular fraction and diffusivity: sensitive to edema, gliosis, and tissue loss.

In this way, a decrease in soma density can be related to neural loss (e.g., medium spiny neurons), and an increase in soma size and extracellular fraction could be related to glial reactivity (astrocytes, microglia). This enables differentiating between atrophy due to neuron loss vs reactive gliosis, which volumetrics or DTI cannot do.

- (4) Integration of modalities: The inclusion of motor impairment (Q-Motor), HD-ISS staging, and multi-compartment diffusion modeling is a methodological strength.
- (5) Early detection potential: SANDI metrics showed abnormalities in premanifest HD, sometimes even when volume loss was mild or absent. This suggests the potential for earlier, more sensitive biomarkers of disease progression.
- (6) Predictive power: Regression models showed that SANDI metrics explained up to 63% of the variance in striatal volumes in HD. And this correlated strongly with motor impairment and disease burden (CAP100). This shows they are not just redundant with volume or DTI, but they are complementary and potentially more mechanistically meaningful.

#### Weaknesses:

Certain aspects of the study would benefit from clarification:

- (1) Scanner and acquisition consistency: While HD data are from the WAND study, it is not clear whether controls were scanned on the same scanner or protocol. Given the use of model-derived metrics (especially SANDI), differences in scanner or acquisition could introduce confounds. Also, although it offers novel and biologically informative markers, widespread clinical translation still faces hurdles. For instance, the study used a 3T Connectom scanner (300mT/m gradients), which is not widely available. Reproduction of these results in standard 3T clinical scanners would be a great addition, in scenarios with lower resolution, less precise parameter recovery, and longer scans if SNR needs to be maintained.
- (2) HD-ISS staging and group comparisons:
- a) Only 26-27 out of 56 gene-positive participants could be assigned HD-ISS stages, and none were classified into stages 0 or 4.
- b) Visual overlap between stages 1 and 2 in behavioral and imaging features suggests that staging-based group separation may not be robust.
- c) The above may lead to claims based on progression across HD-ISS stages to be overinterpreted or underpowered



- (3) Regression modeling choices:
- a) SANDI metrics included in the models differ between HC and HD groups, reducing comparability.
- b) The potential impact of multicollinearity (e.g., between fis and rs) is not discussed.
- c) Beta coefficients could reflect model instability or parameter degeneracy rather than true biological effects.

These issues do not undermine the study's main conclusions, which effectively demonstrate the feasibility and initial clinical relevance of applying SANDI to HD. Nonetheless, addressing them more thoroughly would enhance the clarity and interpretability of the manuscript.

https://doi.org/10.7554/eLife.107661.1.sa2

#### Reviewer #3 (Public review):

#### Summary:

Ioakeimidis and colleagues studied microstructural abnormalities in N=56 Huntington's disease (HD) patients compared to N=57 normative controls. The authors used a powerful MRI Connectom scanner and applied the SANDI model to estimate the soma size, neurite size, soma density, and extracellular fraction in key subcortical nuclei related to HD. In the striatum, they found decreased soma density and increased soma size, which also seemed to become more pronounced in advanced HD individuals in the final exploratory analyses. The authors conducted important analyses to find whether the SANDI measures correlate with clinical scores (i.e., QMotor) and whether the variance of the striatal volume is explained by the SANDI measures. They found a relationship between SANDI measures for both.

# Strengths:

The study is both innovative and of high interest for the HD community. The authors provide a rich pool of statistical analyses and results that anticipate the questions that may emerge in the HD research community. Statistics are carefully chosen and image processing is done with state-of-the-art methods and tools. The sample size gives sufficient credibility to the findings. Altogether, I think this study sets a milestone in the attempts of the HD community to understand neuropathological processes with non-invasive methods, and extends the current knowledge of microstructural anomalies identified in HD with diffusion MRI. More importantly, the newly identified anomalies in soma size and soma density open new avenues for studying these biological effects further and perhaps developing these biomarkers for use in clinical trials.

# Weaknesses:

- (1) An important question is whether the SANDI measures, which require an expensive scanner and elaborate processing, are better biomarkers than the more traditional DTI measures. Can the authors compare the effect size of FA/MD with SANDI measures? In some of the plots and tables, FA/MD seem to have comparable, if not higher, correlations with QMotor or CAP scores. On the same vein, it is unclear whether DTI measures were included in hierarchical stepwise regression. I wonder if the stepwise models may have picked up FA/MD instead of SANDI measures if they are given a chance. Overall, I hope the authors can discuss their findings also in this light of cost vs. benefit of adopting SANDI in future studies, which is an important topic for clinical trials.
- (2) Similar to the above point, it is very important to consider how strong the biomarking signal is from SANDI measures compared to the good old striatal volume. Some plots seem to



indicate that volumes still have the highest correlation with QMotor and the highest effect size in group comparisons. It would be helpful for the community to know where the new SANDI measures stand compared to the most typically used volumes in terms of effect size.

(3) The diffusion measures are inevitably correlated to some degree. Please provide a correlation matrix in the supplementary material, including all DWI measures, to enable readers to better understand how similar SANDI measures are to each other or vs. other DTI measures. Perhaps adding volumes to this correlation matrix may also be a good future reference.

## (4) ISS stages:

- a) The online ISS calculator requires cut-offs derived from the longitudinal Freesurfer pipeline, while the authors do not have longitudinal data. Thus, the ISS classification might be inaccurate to some degree if the authors used the FS cross-sectional pipeline. Please review this issue and see if updated cut-offs should be used to classify participants.
- b) Were there really no participants with ISS 0 among the 56 HD individuals? Please clarify in the manuscript.
- (5) A note on terminology that might be confusing to some readers. According to the creators of ISS, the ISS stages are created for research only; they are not used or applied in the clinic. On the other hand, the terms "premanifest" and "manifest" have a clinical meaning, typically based on the diagnostic confidence level. The assignment of ISS0-1 to premanifest and ISS2-3 to manifest may create some non-trivial confusion, if not opposition, in some segments of the HD community. The authors can keep their current terminology, but will need to at least clarify to the reader that this assignment is speculative, does not fully match the clinically-based categories, and should not be confused with similarly named groups in the previous literature.

https://doi.org/10.7554/eLife.107661.1.sa1

# **Author response:**

# Response to Reviewer 1:

Ad (2) Clinical applications of SANDI have primarily focused on Multiple Sclerosis. However, since the preparation of the manuscript, one study has been published reporting reductions in apparent soma density and white and grey matter differences in apparent soma size in amyotrophic lateral sclerosis (ALS) (https://doi.org/10.1016/j.ejrad.2025.111981). We will include this paper in our revised manuscript.

# Responses to Reviewer 2:

# Strength:

Ad (3) SANDI cannot directly differentiate between neural and glia cells but the pattern of differences in the SANDI parameters we observed in Huntington's disease (HD) are consistent with the known pathology in HD.

#### Weaknesses:

Ad (1) With regards to the question about scanner and acquisition consistency, we can confirm that all diffusion data of individuals with HD and healthy controls from the WAND study were acquired with the same multi-shell High Angular Resolution Diffusion Imaging (HARDI) protocol on the 3T Connectom scanner at CUBRIC. Thus, all diffusion data analysed



and reported in this manuscript were acquired with the same protocol on the same strong gradient MRI system for harmonization and consistency purposes.

We agree that for clinical adoption it is important to demonstrate that HD-related SANDI differences do not require ultra-strong gradient imaging and can be detected on standard clinical MRI systems. While we have not collected such data in people with HD, we and others have demonstrated the feasibility of modelling SANDI metrics from multi-shell diffusion-weighted imaging data acquired with maximum b-value 3,000 s/mm2 on clinical 3T MRI system in typical adults and people with MS or ALS (https://doi.org/10.1002/hbm.26416, https://doi.org/10.1038/s41598-024-60497-6, https://doi.org/10.1016/j.ejrad.2025.111981). These studies have demonstrated that it is feasible to characterise brain microstructural differences with SANDI on clinical scanners and that comparable patterns of results can be observed across different MRI systems. It should also be noted that there is presently a move towards stronger gradient implementation in clinical systems as demonstrated by the release of the Siemens Cima.X system which will allow higher b-value diffusion scanning on clinical systems.

ad (2) We agree that due to the small number of HD participants with HD-ISS staging the exploratory comparisons between ISS stages need to be interpreted with caution. We hope to gain access to some of the missing ISS information and plan to include these in the revised paper.

Ad (3) With regards to the queries about the regression modelling choices:

- (1) As SANDI metrics differed between HC and HD groups, and hence may not be directly comparable, separate regression models for HC and HD data were conducted without formal comparisons between slopes. Only descriptive exploratory comparisons of the observed pattern were included.
- (2) We will provide cross-correlational analyses between all SANDI parameters in the supplements of the revised version of the paper to check for multicollinearity.
- (3)All model-based approaches, including SANDI, may be prone to model instability or parameter degeneracy and we will acknowledge and discuss this in the revised version.

#### Responses to Reviewer 3:

#### Weaknesses:

Ad (1) and (2) The effect sizes (ES) of group differences in SANDI, DTI, and volume measures in the caudate and putamen (Tables 3 and 4) were broadly comparable: apparent soma radius rs (rrb = 0.45 -0.53), apparent soma size fis (rrb = 0.32 -0.45), FA (rrb = 0.38 -0.55), MD (rrb = 0.51 -0.61) and volumes (rrb = 0.49 -0.55). Similar ES were observed between fis and FA, and between rs and volumes. MD showed the largest ES, likely due to striatal atrophy-related CSF partial volume contamination.Cost-benefit analyses of imaging marker choices in clinical trials depend on the aim of the study. DTI provides sensitive but unspecific indices that are influenced by biological and geometrical tissue properties and capture a multitude of microstructural properties. Similarly, volumetric measurements do not inform about the underpinning neurodegenerative processes.

With the advancement of disease-modifying therapies for HD it has become important to identify non-invasive imaging markers that can inform about the mechanistic effects of novel therapies. While DTI and volume metrics are sensitive to detect brain changes, they do not provide specific information about the underpinning tissue properties. Such information, however, may turn out to be important for the evaluation of mechanistic effects of novel therapeutics in clinical trials. Advanced microstructural models such as SANDI may help provide such information. We found that SANDI indices had statistically similar power to the



gold standard measures of volumes, but with the added value of information underpinning microstructure. We and others have also shown that SANDI can be applied to multi-shell diffusion data acquired in a clinically feasible time (~10 min) on standard 3T MRI systems (please refer to our response above).

To summarise, DTI and volumes are sensitive to brain changes but will need to be complemented by more advanced microstructural measurements such as SANDI to gain a better understanding of the underlying tissue changes and effects of disease-modifying therapies.

Ad (3) We will provide a correlation matrix of all DWI measures in supplementary material to allow a better understanding how similar SANDI measures are to each other and compared to DTI measures.

Ad (4) Most of the people with HD who have taken part in our study were participants in the Enroll-HD study. We will use HD-ISS information from ENROLL as much as possible. As we do not have longitudinal imaging data for all individuals classified as ISS <2, we will compare our cross-sectional striatal volumes with those from age and sex matched individuals from WAND to determine whether people fall into ISS 0 or 1 category. This approach will hopefully allow us to increase the total HD-ISS sample size and to determine whether there were participants with ISS 0 in our sample.

Ad (5) We will explain in the revised manuscript that ISS stages are created for research only purposes and are not used or applied in clinic, while "premanifest" and "manifest" are helpful concepts in the clinical context. We will clarify that we refer to individuals without motor symptoms as assessed with Total Motor Score (TMS) as premanifest and to those with motor symptoms as manifest. This roughly corresponds to individuals at ISS 0/1 without signs of motor symptoms compared to individuals at ISS 2-3 with signs of motor symptoms.

https://doi.org/10.7554/eLife.107661.1.sa0